



Review

Coatings and Surface Modification of Alloys for Tribo-Corrosion Applications

Robert J. K. Wood ^{1,*}  and Ping Lu ^{1,2} 

¹ National Centre for Advanced Tribology, University of Southampton, Southampton SO17 1BJ, UK; ad9918@coventry.ac.uk

² Centre for Manufacturing and Materials, Coventry University, Coventry CV1 5FB, UK

* Correspondence: r.wood@soton.ac.uk

Abstract: This review of the tribocorrosion of coatings and surface modifications covers nearly 195 papers and reviews that have been published in the past 15 years, as compared to only 37 works published up to 2007, which were the subject of a previous review published in 2007. It shows that the research into the subject area is vibrant and growing, to cover emerging deposition, surface modification and testing techniques as well as environmental influences and modelling developments. This growth reflects the need for machines to operate in harsh environments coupled with requirements for increased service life, lower running costs and improved safety factors. Research has also reacted to the need for multifunctional coating surfaces as well as functionally graded systems with regard to depth. The review covers a range of coating types designed for a wide range of potential applications. The emerging technologies are seen to be molten-, solution-, PVD- and PEO-based coatings, with CVD coatings being a less popular solution. There is a growing research interest in duplex surface engineering and coating systems. Surface performance shows a strong payoff between wear, friction and corrosion rates, often with antagonistic relationships and complicated interactions between multiple mechanisms at different scale lengths within tribocorrosion contacts. The tribologically induced stresses are seen to drive damage propagation and accelerate corrosion either within the coating or at the coating coating–substrate interface. This places a focus on coating defect density. The environment (such as pH, DO₂, CO₂, salinity and temperature) is also shown to have a strong influence on tribocorrosion performance. Coating and surface modification solutions being developed for tribocorrosion applications include a whole range of electrodeposited coatings, hard and tough coatings and high-impedance coatings such as doped diamond-like carbon. Hybrid and multilayered coatings are also being used to control damage penetration into the coating (to increase toughness) and to manage stresses. A particular focus involves the combination of various treatment techniques. The review also shows the importance of the microstructure, the active phases that are dissolved and the critical role of surface films and their composition (oxide or passive) in tribocorrosion performance which, although discovered for bulk materials, is equally applicable to coating performance. New techniques show methods for revealing the response of surfaces to tribocorrosion (i.e., scanning electrochemical microscopy). Modelling tribocorrosion has yet to embrace the full range of coatings and the fact that some coatings/environments result in reduced wear and thus are antagonistic rather than synergistic. The actual synergistic/antagonistic mechanisms are not well understood, making them difficult to model.

Keywords: tribocorrosion; coatings; surface modification; synergistic effects; wear; corrosion; modelling; experimental; harsh environments



Citation: Wood, R.J.K.; Lu, P. Coatings and Surface Modification of Alloys for Tribo-Corrosion Applications.

Coatings **2024**, *14*, 99. <https://doi.org/10.3390/coatings14010099>

Academic Editor: Yanxin Qiao

Received: 27 November 2023

Revised: 9 January 2024

Accepted: 9 January 2024

Published: 11 January 2024



Copyright: © 2024 by the authors. Licensee MDPI, Basel, Switzerland. This article is an open access article distributed under the terms and conditions of the Creative Commons Attribution (CC BY) license (<https://creativecommons.org/licenses/by/4.0/>).

1. Introduction and Signpost of Reviews

This review focuses on coating and surface modification solutions for applications where tribocorrosion is present. Tribocorrosion can be described as a complex form of material degradation that occurs when a material is exposed to a combination of mechanical

wear and electrochemical corrosion in a tribological contact [1]. Since as far back as 1875, when Edison observed changes in the friction coefficient under different applied potentials [2], it has been widely acknowledged that wear in chemically active environments can differ significantly from wear caused by purely mechanical factors. Similarly, corrosion rates can differ greatly under static, free-surface conditions compared to conditions in which surfaces are also subjected to rubbing or abrasion [3]. The degradation of materials in tribocorrosion is not simply the result of corrosion or wear acting independently but rather involves a complex interaction between both mechanical and chemical factors, which can either work synergistically or antagonistically.

Tribocorrosion therefore is the interaction between wear and corrosion simultaneously. While both temporal and spatial aspects are important, tribocorrosion is often a marriage of not fully understood complex wear processes within the very precise field of electrochemistry and corrosion science. For a comprehensive understanding of the mechanisms and to explain the observed trends, it is essential to consider multiple factors; see Figure 1. These contributing factors are broadly classified into four categories: (1) Mechanical and operational factors: This group encompasses mechanical attributes such as the magnitude of forces, their velocities, the alignment of tribocorrosion, and the geometric shape and size of the components. (2) Electrochemical factors: These include variables such as electrical resistance, the potential applied to the system, and the growth of protective or reactive films on the surface. (3) Surface and coating characteristics: This category covers the material aspects of the system, including the roughness or textural features of the surface, material hardness, and the nature of the wear particles produced. (4) Environmental properties: This group accounts for the conditions of the solution in contact with the material, including temperature, pH, viscosity, concentrations of dissolved oxygen DO_2 and carbon dioxide CO_2 , salinity, temperature, and electrical conductivity. An in-depth understanding of these dynamic material properties provides further insights into the resistance of materials to wear, facilitating a more detailed exploration of how corrosion contributes to material degradation [4]. Experiments should monitor and report on the key factors listed in Figure 1 (surface film, recovery, composition, environment, friction and wear, microstructural changes both on the surface and subsurface, roughness changes, occurrence of electrochemical reaction(s) and so on. This would allow a more generic understanding across the very diverse set of coatings and surface modification techniques being investigated.

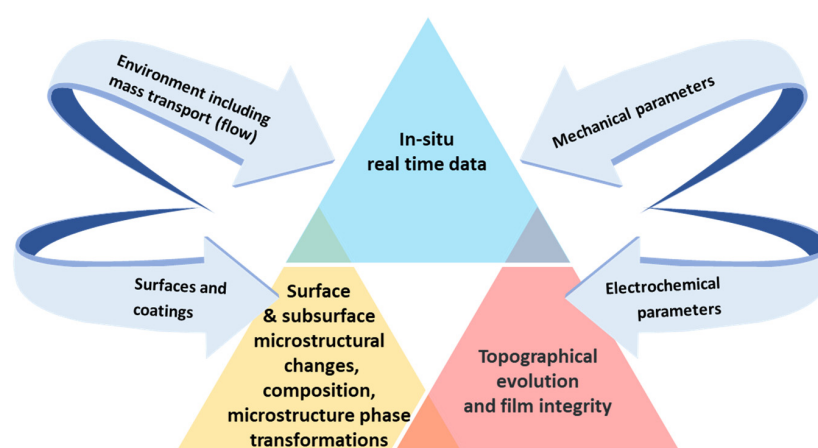
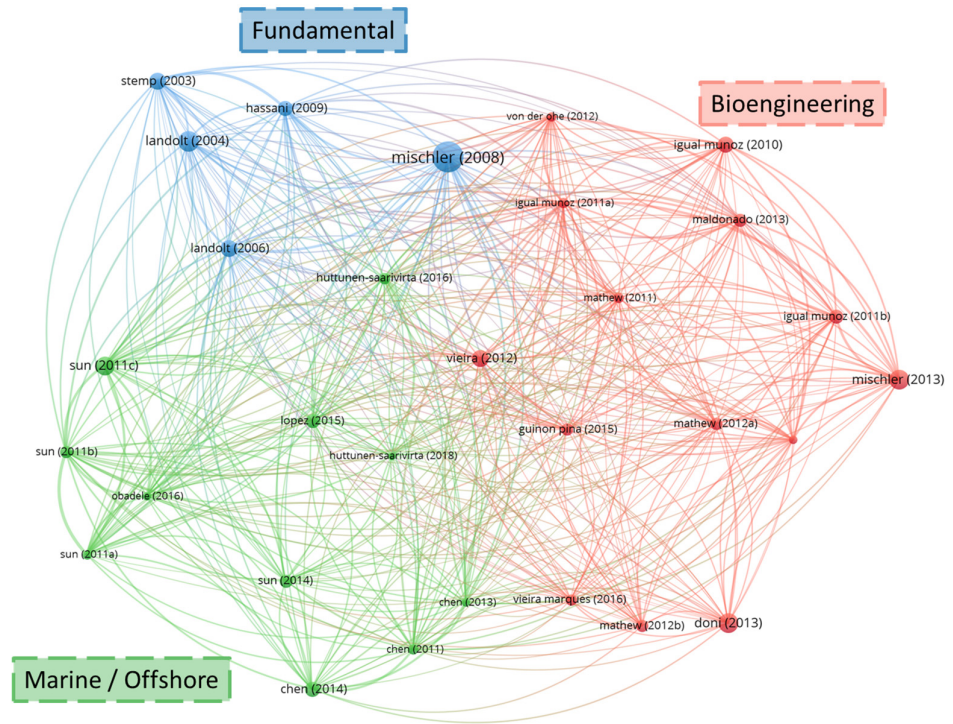


Figure 1. Factors considered in tribocorrosion mechanisms.

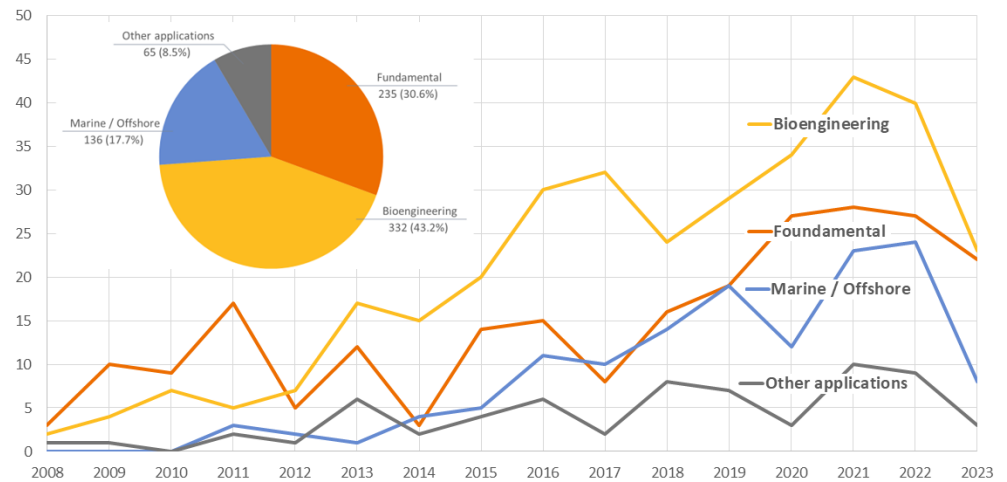
Research trends in tribocorrosion-resistant coatings from 2008 to 2023 were analyzed using a literature survey conducted on the ‘Web of Science’ database, deploying ‘tribocorrosion’ as the targeted keyword within abstracts; this yielded a corpus of approximately 880 scholarly articles on this domain. A deeper insight into this extensive research arena was achieved through a meticulous bibliographic coupling analysis, visualized in Figure 2.

This analytical process, realized utilizing VOSviewer (with the set parameters of full counting, a minimum threshold of 20 citations per document, and a selection of 30 key documents), underscores three main sectors—bioengineering, fundamental studies, and marine/offshore—as the primary focal points within the field of tribocorrosion studies.



(a)

Reported studies (2008–2023) in the area of tribocorrosion based on the web of science searching result



(b)

Figure 2. (a) Identified research clusters: an illustration generated via VOSviewer employing bibliographic coupling for tribocorrosion. (b) Reported studies in the area of tribocorrosion (source: Web of Science search results).

To tackle tribocorrosion effectively, a wide array of surface modification methods have been devised and progressively improved over time. For a thorough exploration of thin-film deposition techniques, readers may refer to a comprehensive review by Abegunde [5]. When selecting coating materials for tribocorrosion applications, it is important to consider

factors such as wear resistance, corrosion resistance, friction, adhesion and compatibility with the substrate material. Figure 3a illustrates a range of surface coating methods [6], and Figure 3b displays various treatment techniques [6–8]. Figure 3c further details the number of papers published on each technique over the years. It is evident that the period from 2019–2023 witnessed a significant increase in publications, particularly in the realm of PEO and PVD techniques. This suggests a growing interest in and preference towards these methods in recent years.

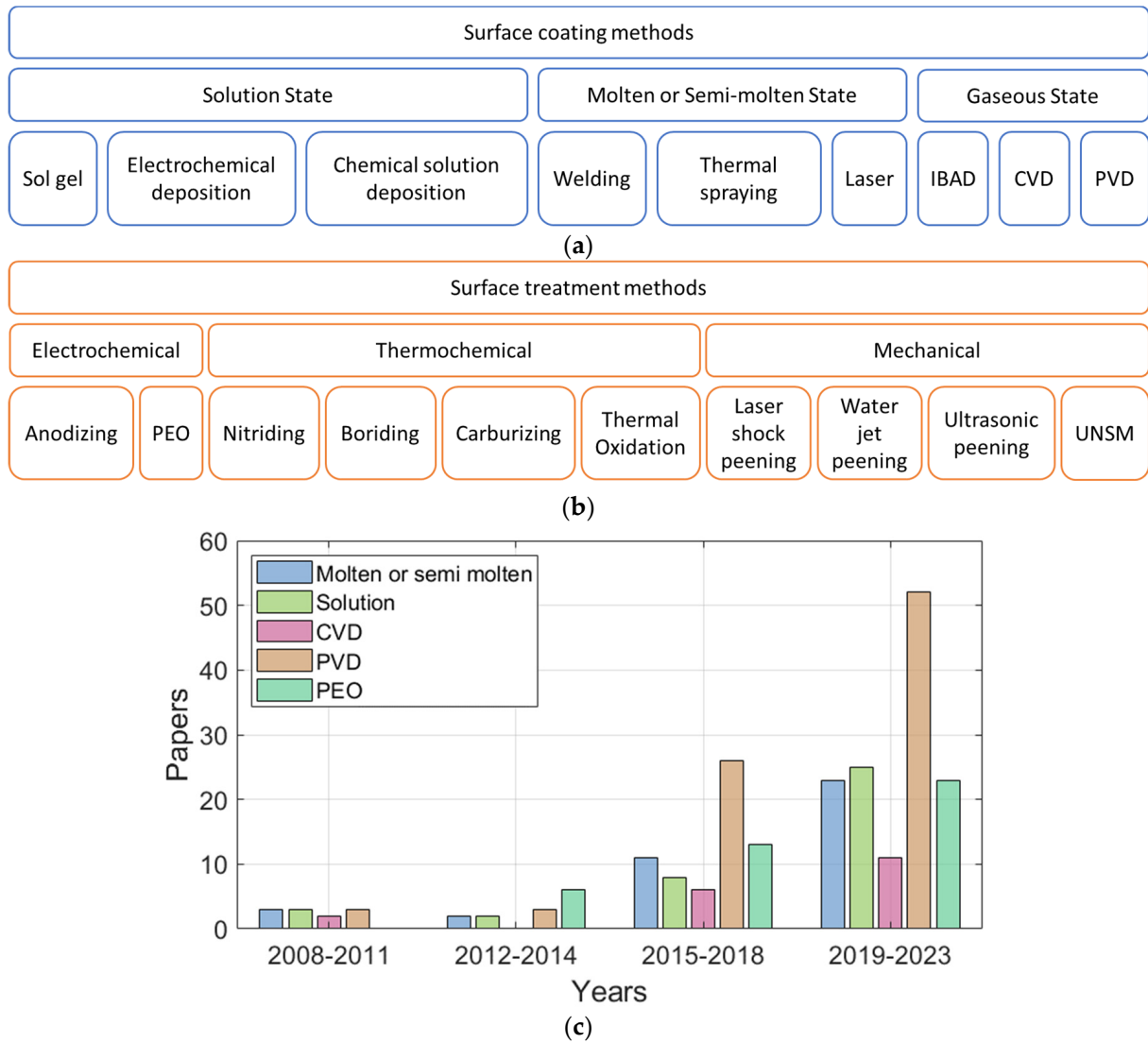


Figure 3. (a) Typical coating techniques, adapted from [6]; (b) surface treatment methods, adapted from [6–8]; (c) papers published using individual techniques.

Wear corrosion interactions [9]:

Under wear corrosion (i.e., sliding or abrasive wear), total damage, T , is given by

$$T = W + C + S \tag{1}$$

where W is the mass loss due to wear, C is the pure corrosion rate and S is the synergistic term. Synergy is defined as ‘the difference between wear-corrosion and the summation of its two parts’ and can be expressed by

$$S = T - (W + C) = \Delta Cw + \Delta Wc \tag{2}$$

Wear can mechanically strip the protective corrosion film, creating fresh (nascent) reactive corrosion sites and producing wear-enhanced corrosion (ΔC_w) [10]. The recovery and inhibition of corrosion is dependent on the rate of repassivation/surface film regrowth and the integrity of the film formed. Tribological stimuli can also change the microstructure (grain refinement), phases (strain-induced transformations) and the integrity of surfaces and subsurfaces (applied stresses induce cracking, for example). The other possible driving mechanisms of ΔC_w are summarized here and include (i) local acidification, (ii) increased mass transport of reactants, (iii) lowering the fatigue strength, (iv) anodic wear scars cathodically polarizing the surrounding unworn surfaces [11] and (v) surface roughening [12]. Corrosion-enhanced wear mechanisms ΔW_c are also possible. The ΔW_c wear rate could be due to (vi) the removal of work hardened surfaces [13], (vii) preferential corrosive attack at grain boundaries [14], (viii) the increase in the number of stress concentration defects resulting from micropitting and (ix) the detachment of plastically deformed flakes on the metal surface due to stress corrosion cracking. Most of the above mechanisms, if dominant, would be expected to lead to positive synergy [9].

Summary of reviews: López-Ortega discussed the evolution of test procedures and standards for assessing the tribocorrosion of passive materials. The work emphasized the adaptation and development of various electrochemical techniques and the importance of understanding the tribocorrosion mechanisms through these methods. A gap identified was the lack of a universal standard that addresses the complexities of tribocorrosion mechanisms, particularly for active materials, which behave differently from passive alloys [2].

The reviews by Mathew T. Mathew and Charlotte Skjöldebrand focused on the critical role of tribocorrosion in biomedical applications, especially regarding implants. Mathew's work laid the foundation by highlighting the challenges in comprehending the complex interactions at play and the absence of a standardized test apparatus. The reviews called for an integrated approach to develop standardized testing methods that can accurately simulate *in vivo* conditions. Furthermore, Mathew's insights pointed to a gap in translational research, emphasizing the need for collaboration to translate laboratory findings into clinical practice [4,15]. Skjöldebrand's review complemented this by examining the current status and potential of wear-resistant coatings for hip and knee implants. The review identified the success of certain coatings, such as TiN and TiNbN, in improving implant properties and reducing the risk of metal ion release and hypersensitivity reactions. However, it also highlighted the critical issue of coating adhesion, which is paramount for the longevity and functionality of implants. Skjöldebrand noted the limited follow-up times and low revision rates, which present a challenge in assessing the long-term performance of these coatings [16]. Additionally, a recent review by Puthillam also delved into the topic of tribocorrosion in biomaterials and its control techniques [17].

The work of Wood provided insights into the tribocorrosion performance of marine materials. The authors' reviews pointed out the lack of understanding of the synergy between mechanical wear and corrosion processes and the need for better prediction models for marine systems. Wood's papers suggested that further research is needed to develop testing facilities with high data acquisition capabilities that can capture the nuanced behaviors of materials under marine tribocorrosion conditions. A potential avenue of further exploration could be to outline methodologies for spatial and temporal analysis that can predict material performance in marine environments more accurately. One might also consider evaluating the efficacy of different coating materials and technologies in mitigating marine wear and tribocorrosion, such as the performance of nickel-aluminum bronze in aggressive ocean environments [18,19].

This review presents a comprehensive overview of the advancements in coating development for tribocorrosion resistance, offering a broad perspective that spans a variety of application domains, from biomedical to marine environments. It serves as a signpost of the recent progress and activities in coatings research, highlighting innovations, challenges, and potential synergies across these diverse fields. While the review may touch on specific

details, it aims to give an overview of trends in recent research, including emerging coating deposition techniques, compositions, applications, testing and modelling.

The review has the following sections: introduction and drivers for research, coating development, modelling, environmental effects, conclusions and remaining challenges.

2. Coating Development

2.1. Coating Techniques (Monolayers)

2.1.1. Molten Deposition

Monticelli looked at thermally sprayed ceramic coatings deposited on steel and exposed to a 3.5% NaCl solution [20]. Coatings prepared by plasma spraying Cr_2O_3 and $\text{Al}_2\text{O}_3/13\% \text{TiO}_2$ powders on a Ni-20Cr bond coat were studied. Due to high levels of porosity, the substrate was not fully protected against corrosion; thus, further work is needed to improve coating quality before being used in tribocorrosion conditions. The same author also looked at the tribocorrosion of PVD magnetron-deposited nanoscale multilayer CrN/NbN coatings deposited on top of thermal spray coatings on steel in 3.5% NaCl solutions [21]. The thermally sprayed coatings were HVOF WC-12Co and Cr_3C_2 -37WC-18Me. They found the PVD top coating offered better tribocorrosion performance of the system, but the coatings degraded over time, and hence this benefit was lost.

Tribocorrosion wear rates of $6.5 \times 10^{-6} \text{ mm}^3/(\text{mN})$ for arc-sprayed AlFeSi metallic glass coatings in 3.5% NaCl (pH 7) solutions reciprocating against 12.7 mm diameter alumina balls under 15N load were reported by Yunyun Ge [22]. Figure 4 compares the wear rates of various coatings under tribocorrosion conditions, as reported in the literature [22–25]. Kuptsov looked at single-layer and multilayer Nb-doped TiC coatings obtained by pulsed arc evaporation (PAE) and electro-spark deposition (ESD) in vacuum and a hybrid approach of the two [26]. Tribocorrosion tests were conducted in air and 3.5% NaCl solution. The single-layer PAE coating demonstrated improved performance and oxidation resistance. The ESD sublayer in the PAE/ESD provided enhanced toughness and increased thickness.

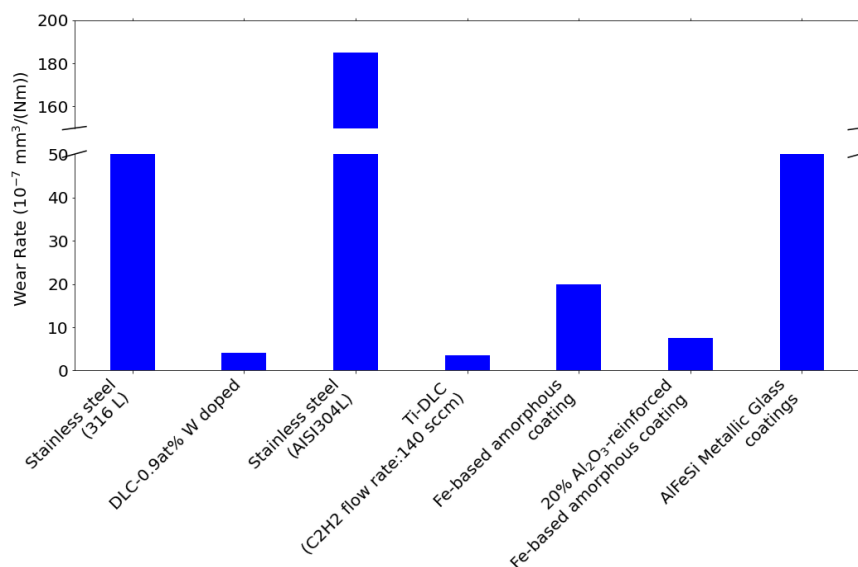


Figure 4. Wear rate for various coatings under tribocorrosion conditions in 3.5% NaCl solution; data from [22–25].

HVOF WC-12Co, WC-10Co4Cr and WC- Cr_3C_2 -7Ni coatings were studied in 3.5% NaCl solution by Kai Hu [27]. The study found that the formation of the CoCr phase on the surface reduced the dissolution of the Co matrix and was not easily removed, making the WC-10Co4Cr coating the most tribocorrosion resistant. Rosanna Pileggi [28] studied HVOF Cr_3C_2 -NiCr cermet coatings and found a strong dependence of the coefficient of

friction on the polarization potential, with a value of 0.28 when the system was under cathodic conditions to a value of 0.11 when under anodic conditions. Rodrigues [29] looked at HVOF Cr₃C₂-25(80Ni20Cr) in double-distilled de-aerated water, 3.5 wt% NaCl, 0.2 M NaOH and 0.2 M H₂SO₄ solutions. The study found that the coating exhibited similar resistance in distilled water, NaOH and NaCl solutions, while the coating showed improved tribocorrosion resistance in H₂SO₄ solutions.

2.1.2. Vapor Deposition

A major deposition route for hard coatings with a thickness of a few to tens of microns is through vapor methods such as Physical Vapor Deposition (PVD) or Chemical Vapor Deposition (CVD). These methods are widely used to improve the electrochemical and thermal properties in the surface performance of various applications, including microelectronics, cutting tools, automotive components and biomedical devices. Recent advancements in hard thin-film coatings for tribocorrosion prevention have primarily focused on two main categories: hard nitride coatings and amorphous carbon (a-C) coatings.

Transition metal nitride coatings, including TiN, CrN, TiCN, TiZrN and TiAlN, are recognized for their hard nitride properties. In a study by Caha, TiN coatings were applied to pure titanium. The impact of various deposition times on the coating performance was analyzed in a 9 g/L NaCl solution maintained at body temperature. The findings indicated that a prolonged deposition time of 80 min resulted in a thicker coating, enriching the percentage of the Ti₂N phase. This enhancement led to an increased resistance against wear [30]. Merl looked at PVD TiAgN and TiSiN hard coatings for protecting stainless steel for biomedical applications [31]. Cui's studies compared the tribocorrosion performance of TiN and TiZrN coatings on Ti-6Al-4V substrate. The TiN coating showed marked chemical stability and an elevated H^3/E^2 ratio, enhancing its resistance to corrosion and wear. The TiZrN coating had wear rates 40%–60% lower than TiN, highlighting the role of zirconium in boosting the properties of the TiN coating [32,33]. Sáenz de Viteri found that the TiCN coating provides excellent protection against tribocorrosion and fretting, as a carbon-rich tribo layer is generated during the sliding process, thereby reducing friction [34]. Tijerina-Gonzalez found that coatings containing oxygen (AlTiON and AlCrON) diminished the porosity and increased the hardness; however, these coatings exhibited higher wear and more damage after tribological tests when compared to AlTiN and AlCrN systems. They also suggest that there is no consistent relationship between the coating hardness or roughness and their adhesion strength or coefficient of friction [35]. Other types of coating including carbide coatings such as TiC, ZrC and TiNbC [36] have been studied by Pana.

Amorphous carbon (a-C) coatings, also known as DLC coatings, have garnered considerable attention since the late 20th century. They are recognized as exceptional protective barriers with excellent hardness, reduced friction and wear, electrical insulation, chemical stability, and biocompatibility [34]. Their proven efficacy in enhancing wear and corrosion resistance has expanded their use, and therefore they play a crucial role in the management of tribocorrosion in various applications [24,37–40].

It was reported by Oliveira that the corrosion resistance could be enhanced up to 59 times compared to the bare SS304 substrate with controlled hydrogen and carbon contents [41]. E. Gracia-Escosa studied TiB_xC_y/a-C coatings deposited on AISI 316L steel in an aqueous solution of 0.26 vol.% acetic acid, 0.16 vol.% peracetic acid and 0.18 vol.% hydrogen peroxide [42]. The corrosion current density of the TiB_xC_y/a-C coating is in the same range as bare steel but with a significantly decreased coefficient of friction (0.1 vs. 0.6) and wear rate (~10 times lower).

Nonetheless, DLC coatings have their own challenges. Hydrogen-free and low-Cr-doped hydrogenated diamond-like carbon (DLC) films on AZ91DMg alloy were studied by Xue-Jun Cui et al., but the results show severe tribocorrosion of the substrate in NaCl solutions; hence, more work is needed to improve coating quality. Wu looked at Cr-doped diamond-like carbon (Cr-DLC) sliding against different counterparts in hydrochloric acid

(HCl); the Cr-DLC film sliding against tetrahedral amorphous carbon (ta-C) showed the best tribological performance [43]. The prevalent high internal stresses and adhesion issues when applied to softer substrates significantly hinder their widespread adoption. Depositing ultrahard coatings on softer substrates can lead to mechanical and chemical property mismatches between the coating and substrate, resulting in high intrinsic stresses and poor adhesion. An additional concern is the presence of defects through the coating thickness [24,44].

To address these challenges, the introduction of metallic elements (Si or N) into the DLC matrix has been explored. This approach involves the formation of a composite structure where metal or metal carbide grains are embedded within an amorphous carbon matrix, effectively mitigating the internal stresses. Subsequent studies have furthered the understanding of DLC coatings. Sun looked at diamond-like carbon (DLC) films with various nitrogen content deposited on TC4 titanium alloys using plasma-enhanced chemical vapor deposition (PECVD) [45]. The effects of the nitrogen content on the tribocorrosion properties in Hanks' solution show that the doped nitrogen induced the formation of new sp^2 sites and generated graphitization in the doped DLC film. The tribocorrosion resistance of the doped DLC film was improved due to the increased adhesion strength and prevented ionic solution permeation. Cui investigated the tribocorrosion properties of a PECVD-deposited multilayer diamond-like carbon (DLC) film doped with Si in NaCl solution [46] and reported lower wear rate in NaCl solution compared to the substrate and a single-layer DLC film. Corrosion and tribocorrosion behavior of super-thick Si-doped diamond-like carbon films deposited by plane hollow cathode PECVD on stainless steel in NaCl solution is reported by Jibin Pu [47]. Three kinds of DLC films with different thickness (4–21 μm) and modulation periods (3–7) were deposited on stainless steel. The tribocorrosion behavior was evaluated in 3.5 wt% NaCl solution using a ball-on-flat tribometer. The life of the film was increased with an increase in thickness, and the tribocorrosion resistance was impacted by the modulation period of the DLC films. The best tribocorrosion resistance of the DLC film was observed with a thickness of 21 μm and using 7 periods.

In a comparative study, Wang and colleagues carefully compared the performance of transition metal nitride coatings and amorphous carbon (a-C) coatings in simulated body fluids (SBFs) [48]. The coatings were deposited on tungsten carbide (WC) discs with a cobalt content of 8.0 at.%, and tribological tests were performed using a pin-on-disc ring against an alumina (Al_2O_3) ball of 8 mm. After a sliding distance of 1000 m, the wear track depths and widths on the coatings were analyzed and compared, as illustrated in Figure 5a. The depths of the wear tracks for the TiAlN, a-C:H and TiN coatings were significantly deep, measuring 2.5 mm, 3 mm and 1 mm, respectively, which exceeded the thicknesses of the films. In stark contrast, the CrN coating's wear track depth was only 0.6 mm, remaining below the film's thickness. The widths of the wear tracks also mirrored the depth trends, with the TiAlN coating exhibiting the widest track at 0.56 mm, and the CrN coating the narrowest at 0.18 mm. Notably, the edges of the a-C:H coating's wear track, highlighted by red frames in Figure 5a, appeared remarkably neat and well-defined compared to the others, which may be indicative of complete delamination under the contact stress experienced during the test. This phenomenon contributed to the high wear rate observed for the a-C:H coating, yet interestingly, the delaminated particles from this coating might have acted as a self-lubricating layer, which is suggested by the relatively low friction coefficient of 0.372.

The further electrochemical analysis depicted in Figure 5b shows that the a-C:H coating displayed the largest capacitive resistance arc in the Nyquist plots, followed by the CrN coating, while the TiAlN coating showed the smallest one. This suggests that the a-C:H coating has a superior ability to resist corrosion in SBFs compared to the other coatings tested. The larger capacitive arc indicates a higher resistance to charge transfer, which could be due to the formation of a more protective passive layer on the a-C:H coating in the corrosive environment of the SBFs.

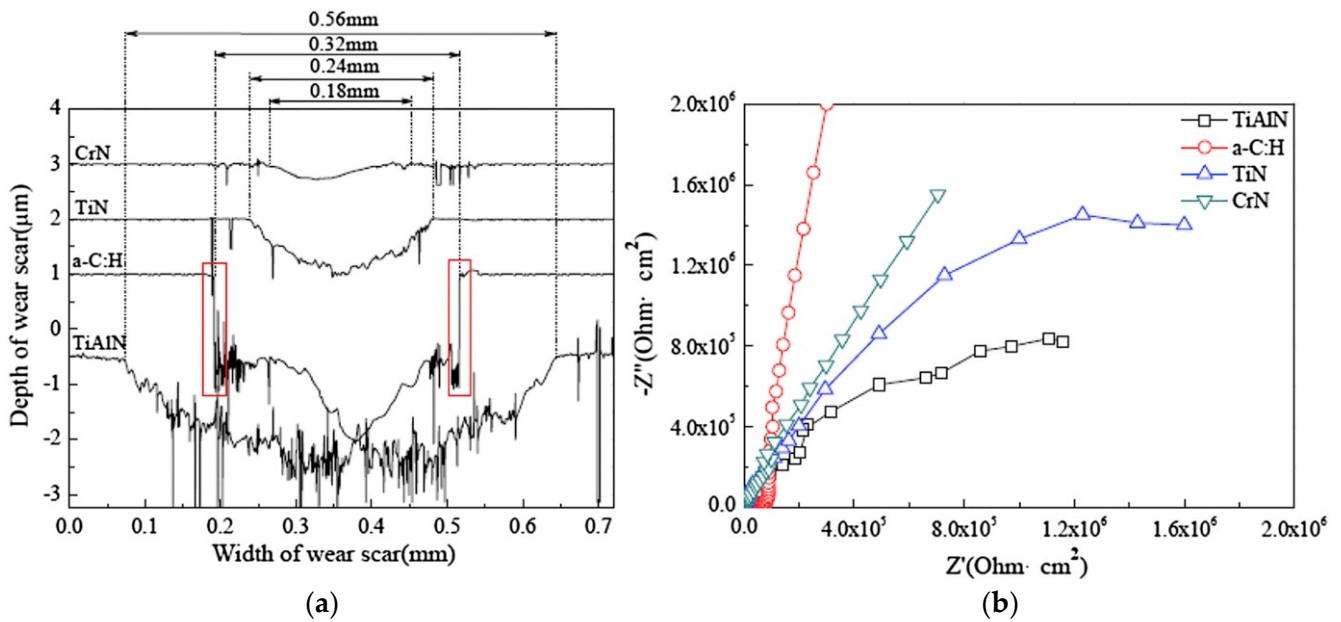


Figure 5. Comparison of different coatings: (a) the cross-sectional contour lines of wear tracks of four types of coatings tested in SBFs, edges of the a-C:H coating's wear track highlighted by red frames; (b) Nyquist plots [48].

Another group of coatings being studied are based on the high-performing refractory high-entropy alloys (HEAs). Four BCC-structured VNbMoTaW and VNbMoTaWCr high-entropy alloy coatings with different Cr contents on 304 stainless steel (304SS) using pulsed DC magnetron sputtering were studied by Luo [49]. Tribocorrosion tests using immersion in a 3.5 wt% NaCl aqueous solution at room temperature under 1 N load and a pin-on-disk tribometer were conducted. Coatings with more than 24.7 at.% Cr exhibited a high hardness range of 16.4 to 16.5 GPa and superior corrosion resistance, both in isolated corrosion and tribocorrosion conditions. The tribocorrosion behavior, particularly at potentials exceeding the breakdown potential, was significantly affected by the protection degradation ratio (Pdr), which is the ratio of polarization resistance in pure corrosion versus tribocorrosion. The lowest recorded wear rate was $2.55 \times 10^{-5} \text{ mm}^3 \text{ N}^{-1} \text{ m}^{-1}$ for the coating with 11.65 at.% Cr, which showed a performance 1.4 times better than that of 304 stainless steel (304SS) under similar conditions.

2.1.3. Deposition from Solutions

Different coatings on a variety of substrates have been deposited by solution techniques for enhanced tribocorrosion protection. In [50], Taşdemir looked at different concentrations of polyurethane and polyvinylpyrrolidone (PVP) blends applied to AISI 316L stainless steel using a dip-coating method. They found that coatings containing up to 25% PVP protected the substrate surface under tribocorrosion conditions induced by reciprocating sliding in a NaCl solution. Ref. [51] looked at sprayed coatings of $\text{Si}_3\text{N}_4/\text{MoS}_2$ core-shell structures and found an enhanced tribocorrosion resistance of the epoxy resin/polyacrylate interpenetrating polymer network organic matrix.

A range of Ni-based coatings have been investigated. In [52], the tribological behavior of electroplated functionally graded nickel- Al_2O_3 nanocomposite coatings produced at different duty cycles in 3.5%wt NaCl solution was investigated. The results show that by decreasing the duty cycle, the width of the wear track decreased due to more particles being incorporated into the coating, changing from a (001) structure to a compact random texture. Although the corrosion resistance decreased by increasing the embedded particles, the increased hardness and compact structure of the coating resulted in better tribocorrosion

properties. A change in the wear mechanism was also seen from adhesive wear for coatings plated at a high duty cycle to the abrasive wear for coatings deposited at a lower duty cycle.

The tribocorrosion of electrodeposited Ni/B coatings was investigated by R. Offoiach [53]. The author found that Ni/B coatings with 0.1 wt% of B are not protective against tribocorrosion due to the presence of cracks in the coating; however, crack-free Ni/B coatings with 0.04 wt% and 0.06 wt% of B show good tribocorrosion behavior with respect to pure Ni coatings. This improved performance is thought to be due to their higher hardness.

The tribocorrosion behavior of the electrodeposited Ni–W coating using a ring-on-block tester was reported by Lee, H.B. [54]. The study reports that columnar grains were embedded with a lamellar and nanocrystalline microstructure in the deposited coatings. The results showed that the wear rate increased as the applied overpotential increased and the surface W-content increased, but the coefficient of friction decreased. XPS analysis determined the surface corrosion film was composed of Ni(OH)₂, NiO and WO₃. The formation of this porous corrosion film at high overpotential was found to cause an accelerated mass loss under tribocorrosion. The tribocorrosion resistance of electrodeposited Ni–Co nanocrystalline coatings in NaOH solution was investigated by Hassani [55]. The author found that adding saccharin into the bath produced a reduced grain size, increased hardness, a change in texture from (2 0 0) to (1 1 1), reduced surface roughness, increased corrosion resistance and improved tribocorrosion behavior.

The tribocorrosion behavior of heat-treated NiP–SiC composite coatings with low particle concentrations was found to be similar to that of NiP coatings. However, for coatings with higher particle concentrations (NiPSiC80 and NiPSC200), the electrochemical properties were compromised, but they had improved wear resistance compared to lower concentrations [56].

Benea, L. studied the tribocorrosion behavior of microstructured ZrO₂–Ni composite coatings using a pin-on-disc in 0.5 M K₂SO₄ solution [57]. The enhanced tribocorrosion properties of ZrO₂–Ni composite coatings were due to ZrO₂ particle dispersion into the nickel matrix, leading to structural improvements and strengthening effects.

Lee Chun-Ying studied electroplated Ni–Mo coatings using a block-on-ring configuration immersed in 5 wt% NaCl solution [58]. Mass loss was increased with applied anodic potential, and minimum coefficient of friction was obtained due to the oxide film. The synergetic effect between wear and corrosion was less significant compared to other Ni-alloys (such as Ni–P, Ni–W and Ni–W–P).

The fretting and wear behavior of Ni/nano-WC composite coatings on stainless steel was studied under dry and wet conditions in [59]. The studies were performed on a ball-on-disk tribometer to simulate the primary water circuit of Pressurized Water Reactors (PWRs), and the results showed that Ni/nano-WC composite coatings displayed a low friction coefficient, high nanohardness, and superior wear resistance compared to pure Ni coatings.

Electrodeposited cobalt–tungsten alloy coatings with a mixed amorphous/nanocrystalline structure were studied by N. Fathollahzade and K. Raeissi [60]. However, they reported that during wear at open circuit potential (OCP), the potential continuously increased to nobler values and then remained at high values even after the end of rubbing. Under anodic polarization, rubbing caused a sharp increase in current density. However, at the end of rubbing, it returned to the initial value. They suggest that mass transport, depassivation, cracking and structure variation played major roles in determining the poor tribocorrosion behavior of the coating.

Nickel oxide nanoparticles ranging from 50 nm to 220 nm were embedded into Ni–P electroless coatings to create a NiO@Ni–P nanoparticle-reinforced composite coating on a brass substrate by Mohammad Reza Rajabi [61]. The study found that increasing the percentage of NiO-NPs in the coating enhances the corrosion and tribocorrosion resistance of the coatings.

A. Salicio-Paz looked at the impact of the multilayer approach on the tribocorrosion behavior of nanocrystalline electroless nickel coatings [62]. The multilayer coatings exhibited

an enhanced tribocorrosion resistance due to the load bearing ability compared to mono-layered ones. Ultrasound-assisted Ni-B coatings have been shown to have tribocorrosion behavior similar to or better than pure Ni coatings [63]. F. Tabatabaei studied the effect of heat treatment on the tribocorrosion of nanostructure Ni-P coatings [64]. High-phosphorus Ni-P coatings were deposited on mild steel and then isothermally heat-treated. Tribocorrosion tests conducted in 3.5 wt-%NaCl solution showed that the maximum tribocorrosion resistance and minimum coefficient of friction was obtained for heat-treated Ni-P coatings at 600 °C.

The tribocorrosion performance of chemically bonded phosphate ceramic coatings (CBPCCs) with different aluminum phosphate (AP) concentrations was studied in [65]. The coating with 35% AP demonstrated the lowest tribocorrosion material loss. The presence of AP improved wear resistance, and the AlPO_4 -coated alumina particles in the coatings enhanced the overall tribocorrosion resistance by altering electrolyte movement during wear and corrosion.

The tribocorrosion protection of Ti-6Al-4V by a composite coating with a plasma electrolytic oxidation layer and sol-gel layer filled with graphene oxide (GO) was reported by Tianlu Li [66]. The addition of GO was seen to improve the tribocorrosion resistance of the PEO/sol-gel film, reducing the wear and acting as a solid lubricant to prevent corrosion in the friction process. Similarly, Bian Da's study shows enhanced tribocorrosion protection from chemically bonded phosphate ceramic coatings (CBPCCs) with added GO-ZnO. The GO-ZnO blocked the electrolyte diffusion pathway, increasing corrosion resistance [67].

While substantial potential is seen in the use of hard coatings, it has also been widely noted that the existence of pores or cracks within such coatings can facilitate the diffusion of corrosive ions, leading to coating failure [68]. Delamination of these single-layered coatings may occur due to the significant hardness difference between the hard coating and soft substrates, which leads to subsequent exposure of the substrate to the electrolyte, significantly decreasing the impedance [40]. Challenges related to the adhesion between the coating and substrate, as well as delamination, remain significant failure mechanisms limiting the use of coatings in vivo. Various clinical case reports indicate that the micro-moving surfaces of recovered TiN-coated joint prostheses used for more than five years' experience spallation and flaking [69]. Consequently, researchers have invested efforts into developing multilayered coatings and duplex treatment processes, recognizing that the interlayer could crucially influence tribocorrosion behavior.

Duplex (thin-on-thick) coating systems formed by thin CrN or DLC layers that are sputter-deposited on top of thick HVOF-deposited Fe_3Al layers on 304-type stainless steel substrates were studied by Fabrice Pougoum [70]. The tribocorrosion experiments confirm that addition of DLC and CrN layers is particularly beneficial when the duplex system is subjected to wear tests during cathodic polarization. However, in the anodic regime, defects formed at the surface are detrimental, as the electrolyte infiltrates the top layer and causes the dissolution of the Fe_3Al interlayer. Kovacı looked at the tribocorrosion properties of duplex surface treatments consisting of plasma nitriding and DLC coating [71]. The effect of damage caused by the synergistic effect of corrosion and wear mechanisms was reduced by the two basic coating parameters of temperature and time. The 600 °C 4 h + DLC coating exhibited the best tribocorrosion resistance. Bayón studied the effect of repassivation on the tribocorrosion performance of two types of multilayer coatings: one with alternating Cr and CrN layers, and another with layers of CrN and ZrN [72]. The study found that while the friction force does not directly affect tribocorrosion, wear processes do. A phenomenological model for the repassivation of these coatings was established, which correlates the rate of mechanical activation caused by friction with the behavior of the open-circuit potential.

Numerous multilayered coatings for biomedical applications have been proposed in the literature. One strategy aims to further enhance the coating hardness and address single layer defects. Bai's research demonstrated that the incorporation of Ta- or Ti-doped multilayered structures onto Ti-6Al-4V alloy enhances the tribocorrosion resistance of a-C

films, providing them with improved wear and corrosion resistance compared to both the single-layered a-C film and Ti-6Al-4V [73]. Comakli investigated the surface hardness of a TiN/TiAlN multilayer and found that the maximum hardness was reached for TiN/TiAlN multilayer-coated samples [74]. Caha's research determined that, although the TiN coating did not enhance the tribocorrosion resistance of Ti-12Nb alloy due to the coating delaminating, applying a ZnO layer on top of the TiN coatings significantly improved performance by increasing microhardness and providing a robust physical barrier [75]. CrN and CoCrMo carbon S-phase layers were systematically studied by Bertram Mallia's group [76–78]. Among these, CrN/S coatings on 316L demonstrated remarkable tribocorrosion resistance, attributed to their high hardness and substrate adhesion.

Another approach is to use a combination of the hard and brittle nitride coatings, with a softer metal (Cr, Ti, Ta and Zr) as an interlayer, which is recommended to manage interfacial stress and to avoid crack growth. The use of Ti/TiN was studied by Naghibi [79] and Zhao [80]. Zhao showed that the tribocorrosion resistance of multilayered coatings was increased approximately two times compared with the single-layered TiN coating. Recently, the study by Beliardouh applying $(\text{Ta}/\text{ZrN})_n$ on Ti-6Al-4V evidenced that the synergistic effect leads to complete deterioration of the multilayer coating. The coating's architectural thickness design is critical (see Figure 6), and the elasto-plastic properties of the adjacent surfaces are a key factor in the wear mechanism [81].

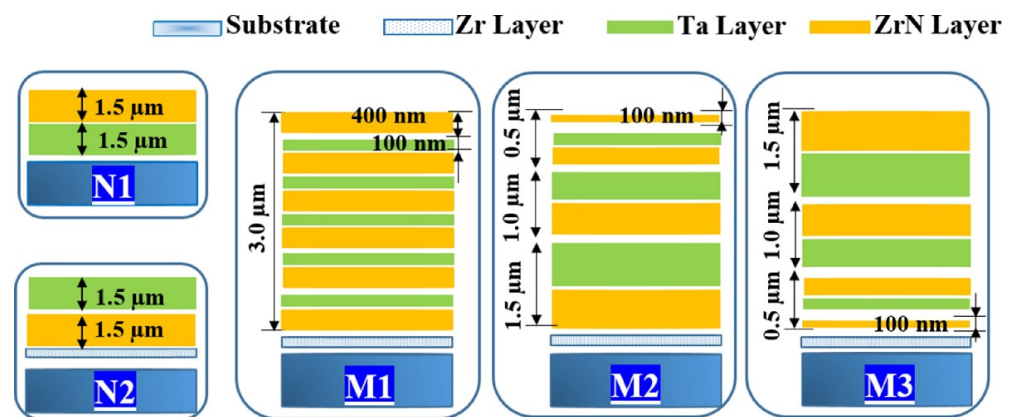


Figure 6. Gradient multilayer coatings [81].

Recently, duplex layered coatings, which encompass a hybrid technique involving an initial thermo-chemical treatment (such as oxidation, nitriding or carburizing) followed by a subsequent film deposition process, have attracted substantial research attention. Frutos looked at nitrogen diffusion layers, achieving a thickness of up to 12 μm, followed by the application of a CrN coating through PVD. The findings reveal a substantial enhancement in surface hardness, increasing it by a factor of 5.5, while also exhibiting a marked reduction in both pitting susceptibility and wear volume loss compared to untreated counterparts [82]. Zhao evaluated the effects of plasma nitriding and DLC surface modifications on three different substrates, discovering that nitrided SS316 and CoCrMo negatively impact tribocorrosion performance, while plasma nitriding on pure Ti produces a thick, dense and homogeneous TiN layer similar to the DLC coating [83]. Conversely, Uzun found that a duplex surface-treated sample on SS316 improves performance instead of exhibiting negative effects [84]. Grabarczyk studied the effects of oxidation or carburizing prior to the DLC coating deposition on Ti-6Al-4V, indicating that a two-step modification of oxidation followed by DLC coating yielded optimal outcomes [85]. In general, the adequate combination of thermo-chemical treatment and coating deposition can significantly improve tribological and corrosion properties, while the parameters set for the treatment process determine the resulting phases and further impact the final performance.

PEO, or Plasma Electrolytic Oxidation, has emerged as a significant topic of research and industrial application, particularly gaining momentum from the 2010s onward. This

process, used to create oxide coatings on lightweight metals such as aluminum, titanium, and magnesium, generates enhanced wear resistance, improved corrosion resistance and increased surface hardness. These coatings have been found to promote bone ingrowth and ensure stable implant fixation, marking them as crucial developments for biomedical implant materials. Creating a thin organic/inorganic layer on a PEO coating is an attractive method and has been considered by many researchers. A comprehensive study by A. López-Ortega using PEO demonstrated the potential for creating ceramic-like oxide layers on titanium alloys, enhancing wear-corrosion resistance and cell adherence, which are crucial for successful osteointegration. These layers were modified with various elements to enhance osteointegration and provide antibacterial properties [86]. A series of composite coatings were developed on Mg alloys and Zr alloys to enhance their properties.

Table 1 summarizes the characteristics and preparation methods of these coatings, showcasing a range of approaches and their effectiveness as determined through various tests.

In addition to the advancements in Plasma Electrolytic Oxidation (PEO), the boriding process emerges as another notable surface modification technique. Specifically, TiB₂ + TiB coatings were formed on Ti-6Al-4V through a molten-salt diffusional process at temperatures of 850 °C and 900 °C for 16 h by Rahmatian [87]. The research highlights that at a higher temperature of 900 °C, the TiB layer's thickness increases significantly, enhancing the material's wear resistance. This process results in a substantial decrease in the tribocorrosion rate, demonstrating a 98% reduction compared to uncoated Ti-6Al-4V after enduring 36,000 cycles of sliding under a 15 N load. However, the borided layers applied at 850 °C showed complete wear, indicating the critical role of temperature in this process.

Another surface modification method is laser shock peening (LSP). A Ti₄₀Zr₂₅Ni₃Cu₁₂Be₂₀ bulk metallic glass (BMG) was treated by laser shock peening 1, 2 and 30 times, leading to internal structural changes and the generation of free volume [88]. This process improved the BMG's plasticity and crack resistance and increased its surface microhardness. The average tribocorrosion volume loss rate of the LSP specimen decreased by approximately 11%. However, excessive LSP caused increased surface roughness (552.9 nm), which made the surface more prone to pitting and reduced its tribocorrosion resistance.

Table 1. Summary of research on PEO techniques applied to Mg and Zr alloys.

Substrate	Tech	Solution	Test	Findings	Ref.
AZ31B Mg alloy	PEO with pullulan	SBF	EIS, OCP, PDP	An optimal pullulan concentration is determined in the silicate-based electrolyte solution for achieving the best anti-corrosion properties in the PEO-treated alloys. Specifically, the corrosion resistance improved as the pullulan concentration increased from 0 to 1.0 g/L.	[89]
AZ31B Mg alloy	PEO + CS dip	SBF	EIS, OCP, PDP	The PEO-treated AZ31B Mg alloy is porous and has multiple micro-cracks. Using hydrothermal treatment (HT) leads to the precipitation of Mg(OH) ₂ crystals over the PEO sample. When a chitosan (CS) layer was applied on top of these treated samples, it effectively sealed the pores and cracks. As a result, the combination of PEO, HT and CS coatings significantly enhanced the corrosion resistance of the Mg alloy, as evidenced by the order of anti-corrosion properties: PEO/HT/CS > PEO/CS > PEO/ HT > PEO > substrate.	[90]
Zr-2.5 Nb alloy	PEO (ZrO ₂ -Al ₂ O ₃)	PBS	EIS, OCP	The main wear mechanism for the uncoated Zr-2.5 Nb alloy substrate was identified as adhesion, with wear particles adhering to the surface locally. In contrast, for the coated surfaces, delamination was the predominant wear mechanism, signifying a significant improvement in wear resistance for the coatings.	[91]

Table 1. Cont.

Substrate	Tech	Solution	Test	Findings	Ref.
AZ31B Mg alloy	PEO with multi-walled carbon nanotubes	SBF	OCP, PDP	The presence of MWCNTs induced the formation of Mg_2SiO_4 in the coating, in addition to the already existing MgO. The reinforcement with MWCNTs led to a 15% reduction in the coefficient of friction and decreased wear-related damage by 60%. Moreover, the corrosion resistance of the coating was enhanced, especially against pitting corrosion.	[92]
AZ31B Mg alloy	MAO Ca/P coating	SBF	EIS, OCP, PDP	The magnesium alloy, when treated with ultrasonic cold forging technology (UCFT) followed by micro-arc oxidation (MAO) containing calcium phosphate, demonstrated superior tribocorrosion resistance. When friction was applied to the samples, there was a significant increase in corrosion.	[93]
AZ31B Mg alloy	Si, Si + P, Si + B	SBF	EIS, OCP, PDP	The microstructure and surface morphology of the MAO coatings were found to be similar, with all having an outer porous layer and an inner dense layer. Among the various coatings, the one produced with both Si and B (Si + B) in the electrolyte was the thickest and exhibited the highest hardness.	[94]

3. Modelling

Modelling tribocorrosion requires mechanical wear and electrochemical corrosion components, and their interaction creates a synergy or antagonism between the two processes; see previous sections on wear-corrosion interactions. Thus, modelling needs a way to accommodate surface damage, the removal of protective surface films and the rate of regrowth. Modelling synergy/antagonism between wear and electrochemical processes allows prediction of the total surface removal. Synergy has a ΔW_c (corrosion-enhanced wear) and a ΔC_W (wear-enhanced corrosion) component. Recent modelling and mapping papers that address tribocorrosion are shown in Table 2. As can be seen, many papers look at passivating metals and use finite element models (BEM/FEM), or look at affected areas (galvanic model) of sliding and use a form of the Archard wear law and mechanically (wear) accelerated corrosion/electrochemical equations (i.e., Tafel, Landolt, Mott-Schottky and Faraday's equations) or COMSOL for current density modelling, to predict the tribocorrosion loss from the surface [95–103]. For instance, one study compared the tribo-electrochemical Open Circuit Potential (OCP) experimental curve with mathematical simulations for Stellite samples in 0.5 M H_2SO_4 ; see Figure 7. Landolt's wear-enhanced corrosion model, which incorporates the repeated removal of the passive film within the contact area, is depicted in Figure 8 [104]. One model combines this with a lubrication model; see Figure 9 [105]. Distribution of the current density of electrolytes on various electrodes is calculated and presented by Miyabe [106]; see Figure 10. Care should be taken when using Faraday's law to convert current into volume loss, considering the exact electrochemical reactions occurring and the number of electrons being transferred. Other models look at passive metals undergoing plastic deformation at asperity scales that accommodate micro-shearing and low cycle fatigue. Depassivation at asperity contacts can be summed to model quantification of total corrosion current. More advanced modelling for cycle loading effects seeks to model the interaction of applied fatigue and tensile stresses, based on corrosion fatigue (CF) and stress corrosion cracking (SCC) mechanisms [107,108]. One paper uses DFT to look at the origins of corrosion [109].

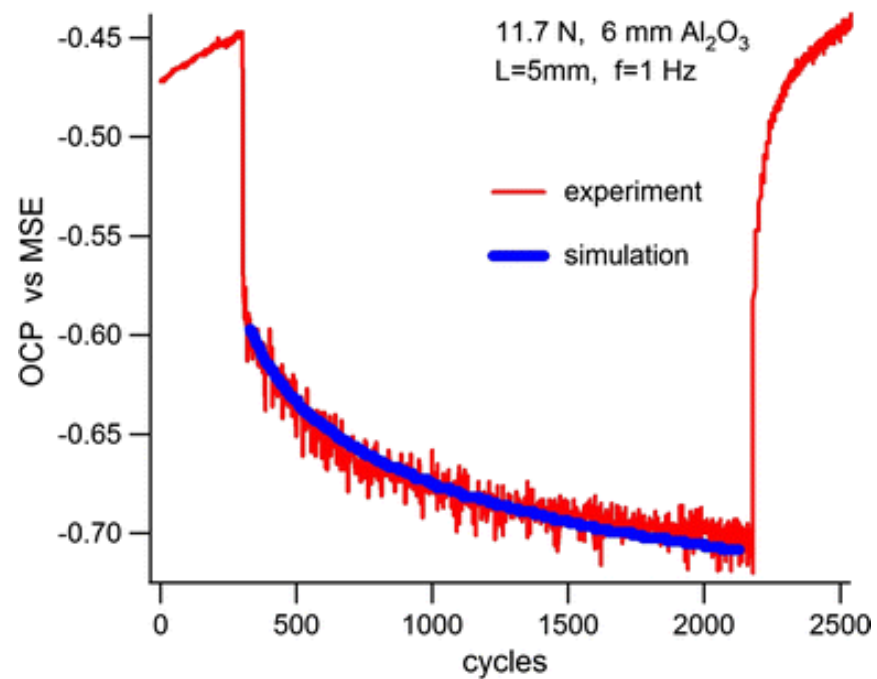


Figure 7. Tribo-electrochemical OCP experimental curve and the mathematical simulation (superposed) for the stellite 21 sample in 0.5 M H_2SO_4 at 11.7 N normal load, showing the close agreement of the OCP evolution prediction with the experimental response [99].

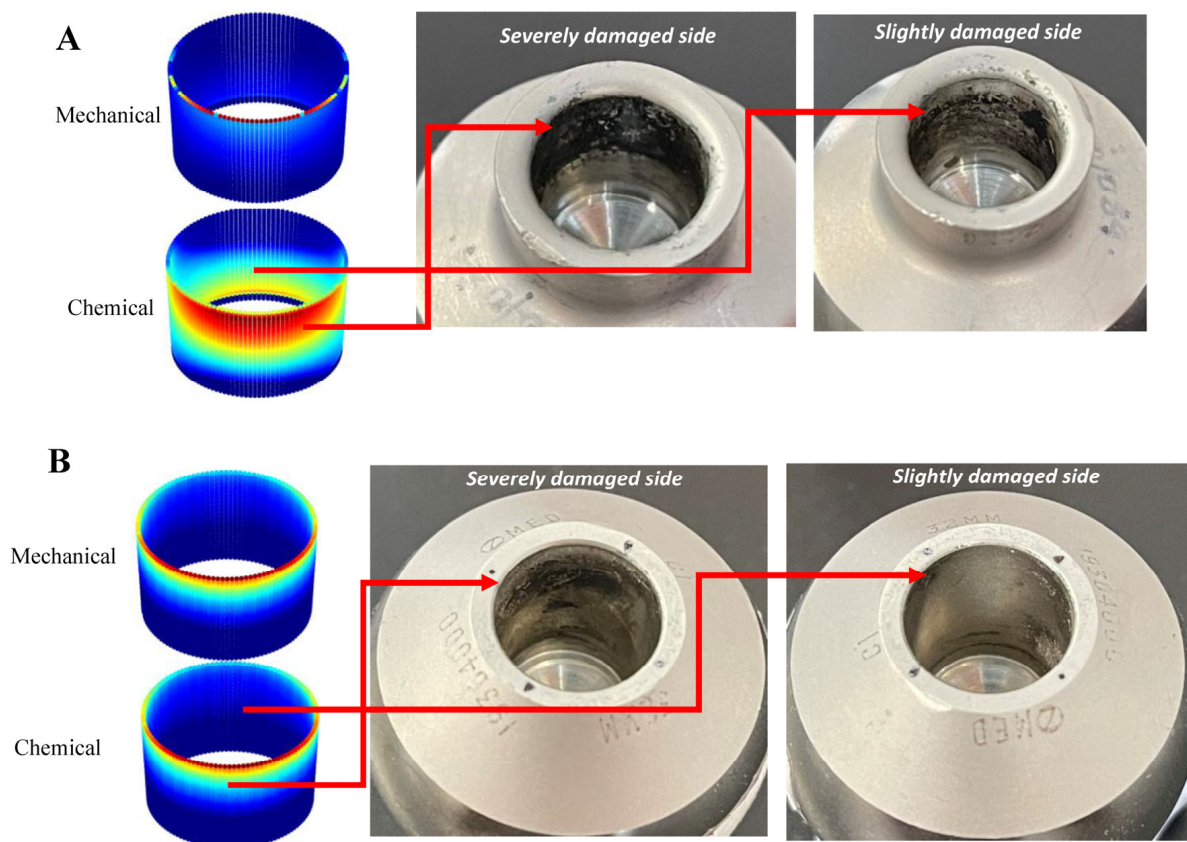


Figure 8. Comparison between the tribocorrosive wear profiles on the head tapers between the FE model and retrieved samples with different levels of assembly force: (A) less than/equal to 2 kN, (B) more than/equal to 4 kN [104].

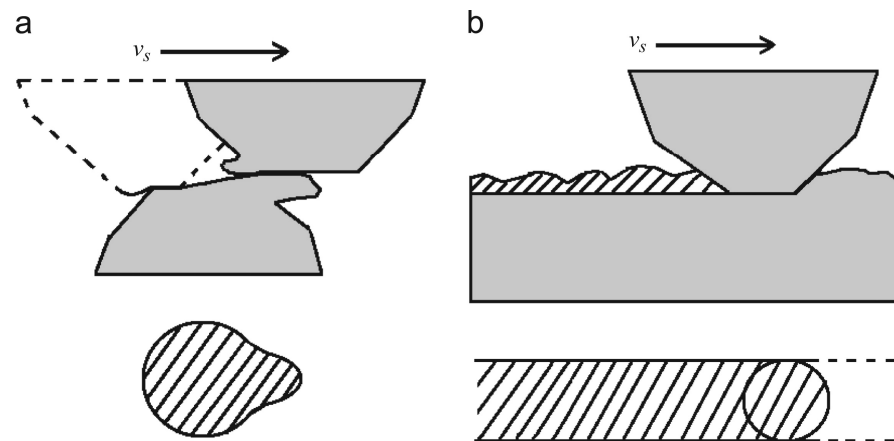


Figure 9. Schematics of the contacts between asperities (a) or between asperity and flat counter body (b). Dashed areas represent plastically deformed and then depassivated metal surfaces [105].

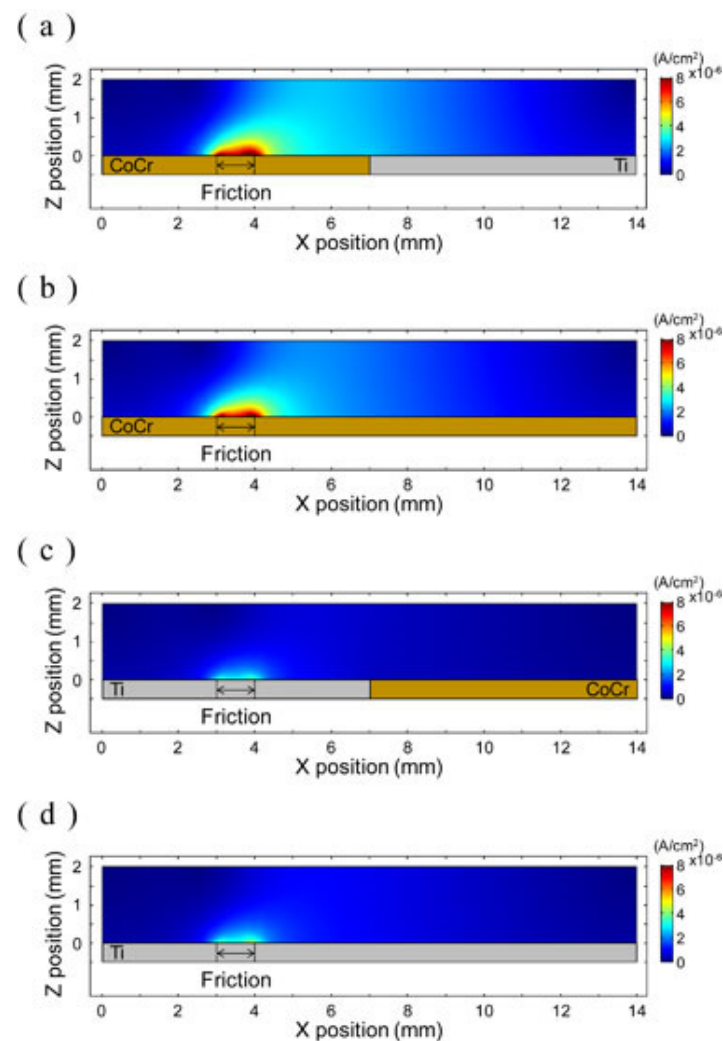


Figure 10. Distribution of current density of electrolyte on various electrodes. (a) CoCr(Tribo.)–Ti model, (b) CoCr(Tribo.) model, (c) Ti(Tribo.)–CoCr model and (d) Ti(Tribo.) model [106].

One model uses the kinetics for interface-limited film growth to find analytical expressions for the current transients, including the conductivity and pH of the electrolyte as well as the contribution from the confined geometry within the mechanical contact [110,111].

The corrosion-enhanced wear aspects of synergy were not modelled until recently, when a deterministic model calculated the corrosion-enhanced wear (ΔW_c) and proposed that changes in the topography are responsible for this synergistic effect [103,112]. Only one paper was found that models the tribocorrosion of coatings [109]. Tribocorrosion mapping using machine learning is reported in [113–116], which use experimental data to predict regimes of degradation; see Figures 11–13. The low-cycle micro-fatigue wear affected by corrosion was modelled by Jiang [117]; see Figure 14.

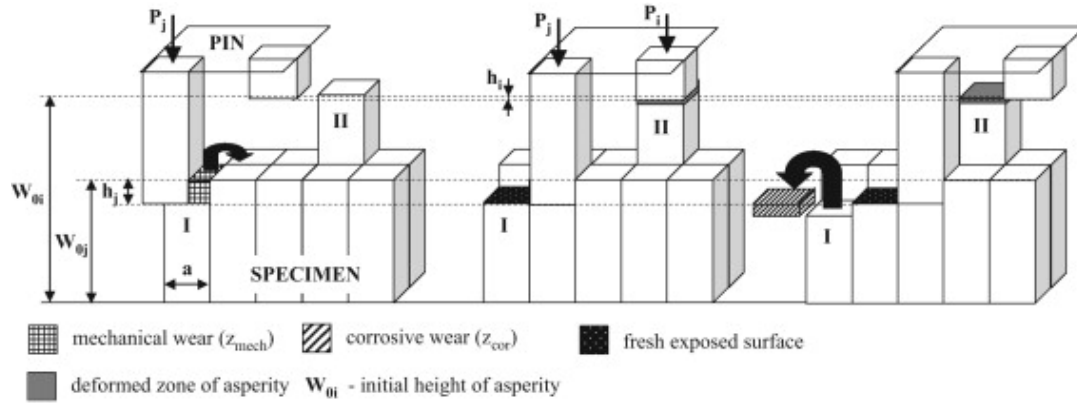


Figure 11. Model of the tribosystem [113].

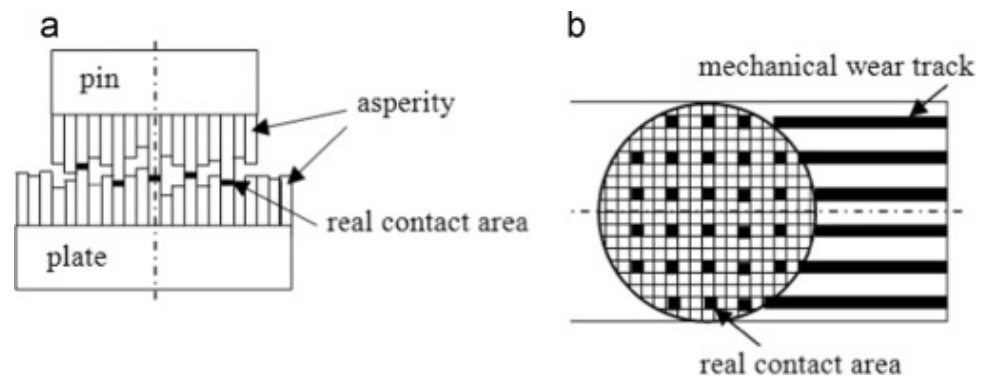


Figure 12. Computational model: (a) axial cross-section of the pin-on-plate combination, (b) nominal contact area beneath the pin [114].

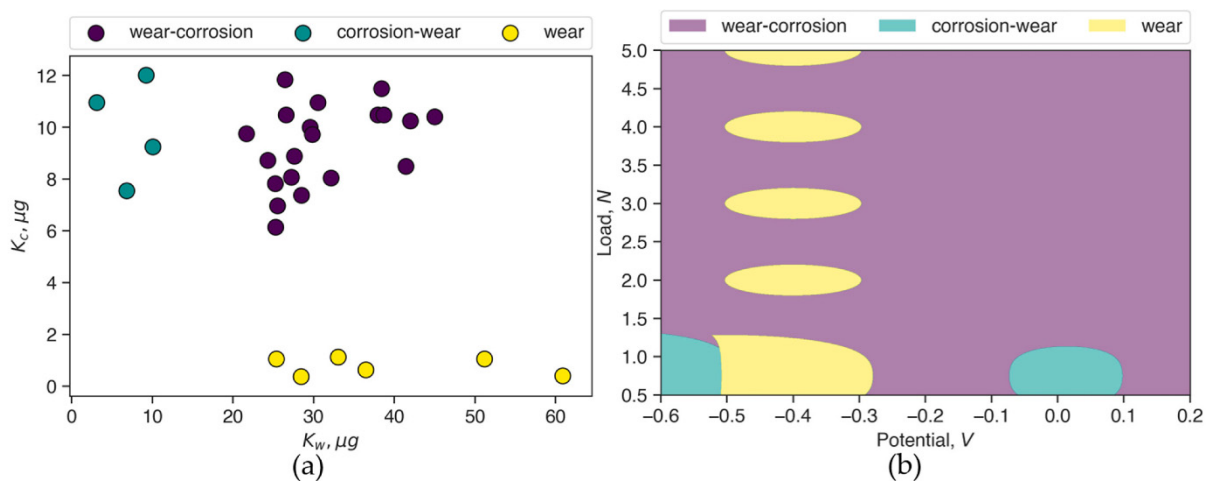


Figure 13. (a) Three clusters in dataset 2 identified using K-means clustering and (b) the tribocorrosion mechanism map of Co-Cr generated using SVM [116].

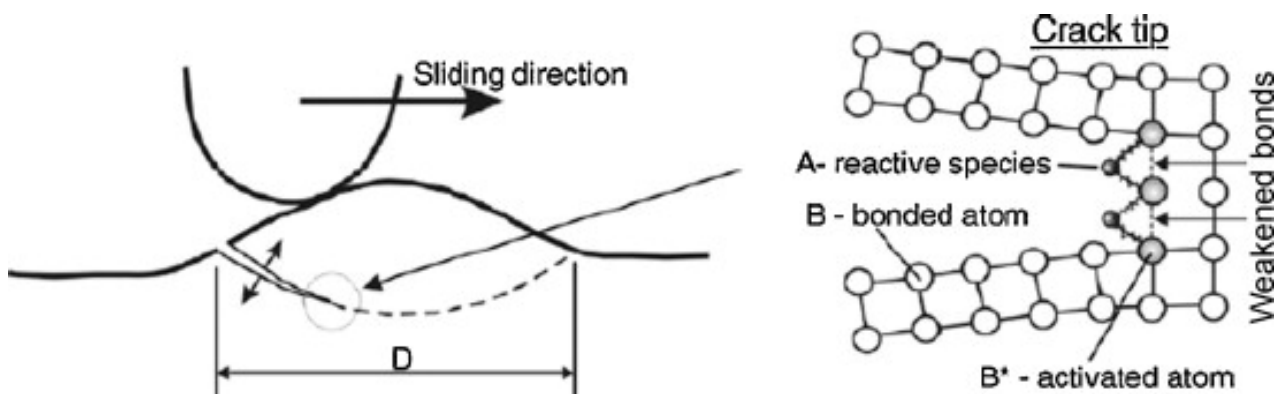


Figure 14. Low-cycle micro-fatigue wear affected by corrosion [117].

The modelling of tribocorrosion has yet to embrace the full range of coatings and the fact that some coatings/environments result in reduced wear and thus are antagonistic rather than synergistic. The actual synergistic/antagonistic mechanisms are not well understood, making modelling difficult; these need to be fully understood to enable modelling to advance. However, models developed for bulk surfaces, as discussed above, are applicable but are themselves still under development. Other areas that need to be included are the role of debris in the contact, temperature/flash temperatures, areal roughness evolution, the chemistry of oxides and corrosion reactions, complete and partial film removal and growth rates, porosity and defects, microstructural and compositional evolution, selective phase corrosion attack, environmental changes in the interface, strain hardening/phase transformations, material transfer between mating surfaces, the porosity of coatings and subsequent permeation of electrolytes to the coating–substrate interface, interfacial corrosion/cathodic disbondment, galvanic coating–substrate interactions, the role of corrosion products, and intrinsic residual and surface stresses. Table 2 shows the papers with a focus on modelling tribocorrosion and the approaches they have taken. Although few focus on coatings, the bulk surface models show a way forward and demonstrate the coupling between mechanical and electrochemical approaches and the platforms (e.g., FEM, multi-physics, machine learning/neural networks) needed for modelling coatings. Examples of the different contact scales and approaches are given in Figures 7–14.

Table 2. Modelling summary.

Model	Technique	Validation	Ref.
Wear maps	Rough asperities are represented as a system of adjacent cuboids. Each cuboid refers to one asperity to explore levels of deformation and stress. Two mechanisms of asperity wear are considered: micro-shearing and low cycle fatigue.	Repassivation of AISI 304 steel in a 0.5 M solution of H ₂ SO ₄	[114]
Modelling the evolution of the electrochemical current in the potentiostatic condition using an asperity-scale model of tribocorrosion	This is an asperity-scale electrochemical model coupled to a computational contact mechanics solution. It models the real-time evolution of surface topography, wear and corrosion.	The model determines the micro-scale current, and the summation of these currents defines the macro-scale quantity of the current. This model was validated with experiments using a ball-on-plate tribometer.	[103]

Table 2. Cont.

Model	Technique	Validation	Ref.
A New Asperity-Scale Mechanistic Model of Tribocorrosive Wear: Synergistic Effects of Mechanical Wear and Corrosion	A corrosive wear model is considered at the asperity scale and coupled with a traditional Archard-type mechanical wear model. The geometry of the surface asperities is modified in a contact mechanics model. This deterministic model calculates the corrosion-enhanced wear.	This work studied CoCrMo as the working electrode (WE) and the Si ₃ N ₄ ball as the counter body in a reciprocating configuration. Contributions of total mechanical wear and corrosion suggest that wear-enhanced corrosion was a significant contribution in the overall degradation of the material.	[112]
Predictive wear model based on a mechanistic approach of tribocorrosion and lubrication and taking into account clinically relevant parameters such as normal load, velocity and clearance	Passive metals are considered that allow for plastic deformation at asperity contacts, combining mechanical wear (Archard's law), chemical wear (wear-accelerated corrosion) and hydrodynamic lubrication.	Good agreement with wear rates observed in tribometers and the running-in wear rate of artificial hip joints tested in simulators	[105]
Time dependence of the material degradation mechanisms	BEM/Archard	AISI316L in a 3% NaCl solution	[95]
Tribocorrosion mechanisms of NiCrMo-625alloy: electrochemical modelling	Archard plus electrochemical model	Experimentally validated	[96]
Hip joint stem interface modelling	An adaptive finite-element-based model using a combination of Landolt's passive film equation and Faraday's law, in parallel with Archard's wear model to simulate fretting corrosion	This model was able to predict the damage pattern at the retrieved head-neck interface.	[104]
Finite element-based simulation of tribocorrosion at the head-neck junction of hip implants	Finite element (FE) model for the head-neck junction of hip implants. Archard wear equation and Maldonado electrochemical model used [118]	The FE-predicted wear patterns were comparable with those observed in retrieved tapers.	[98]
In situ determinations of the wear surfaces, volumes and kinetics of repassivation: contribution to the understanding of the tribocorrosion behavior of a ferritic stainless steel at various pH levels	Wear model using Archard's law; however, a non-linear dependence of Archard's coefficient with pH is seen. The role of pH in influencing the film regrowth kinetics is shown.	The film reactivity depends on pH; tribocorrosion experiments were performed on ferritic stainless steels in sulphate solution (pH 1.5, 6.5 or 12.5).	[103]
Electrochemical Simulation of the Current and Potential Response in Sliding Tribocorrosion	Combined Tafel, galvanic (wear/surrounding area) and Archard equations	Excellent agreement of experimental wear data and the experimental OCP curves	[99]

Table 2. Cont.

Model	Technique	Validation	Ref.
Area-dependent impedance-based voltage shifts during tribocorrosion of Ti-6Al-4V biomaterials	An area-dependent Randle's circuit is used with the tribocorrosion current equation. The potential drop over time depends on the surface impedance characteristics, the area of the electrode, the material and the mechanical conditions, giving rise to the oxide film abrasion. It accounts for the effects of oxide film onset potential, the voltage dependence of the oxide film properties and repassivation, and galvanic effects. The model also incorporated voltage-dependent circuit elements such as the Tafel and the Mott-Schottky elements to account for the changes in these properties with voltage.	Experiments use titanium pin-on-disc fretting corrosion	[101,102]
Modelling nanostructured metallic multilayers	A finite element (FE)-based computational model and density functional theory (DFT) calculations.	Nanomechanical and electrochemical measurements were coupled with advanced material characterization tools.	[109]
Multiphysics modeling and uncertainty quantification of tribocorrosion in aluminum alloys	Finite element-based multiphysics model. Two surrogate models, Gaussian process and neural network with dropout, were used for uncertainty quantification of the finite element model.	Validated by existing tribocorrosion experiments of two Al alloys	[97]
Tribocorrosion of CoCr Alloy and Ti with Galvanic Coupling in Simulated Body Fluid	Numerical simulation of current density distributions conducted with COMSOL Multiphysics 5.3 software	Experimental results	[106]
Modelling Current Transients in a Reciprocal Motion Tribocorrosion Experiment	Kinetics for interface-limited film growth were used to find an analytical expression for the current transients. This included the conductivity of the electrolyte as well as the contribution from the confined geometry within the mechanical contact.	Good experimental fit over a range of electrolyte conductivities and with electrochemical impedance spectroscopy	[110]
Growth mechanism and repassivation kinetic determinations on stainless steel under sliding: Role of the solution pH and dissolved oxygen concentration	Higher wear rates were measured in low pH and aerated solution. Temporal analysis of the transients showed faster passivation of the wear track in acidic solution.	The degradation rate was correlated to the passivation kinetic.	[111]
Machine Learning Model to Map Tribocorrosion Regimes in Feature Space	Unsupervised machine learning is used to identify and label clusters from tribocorrosion data. The clusters are used to train a support vector classification model, which is used to generate tribocorrosion maps.	The generated maps are compared with those from the literature.	[115]
Applicability of a recently proposed tribocorrosion model for CoCr alloys with different carbide content	Dowson model for mechanical and electrochemical wear [119]	Validated by tests on Stellite 6 and Stellite 21	[100]

Table 2. Cont.

Model	Technique	Validation	Ref.
Fully Coupled Tribocorrosion Simulation Method for Anchor Chain, Considering Mechano-Electrochemical Interaction	Fortran model, where both stress-accelerated corrosion and corrosion-accelerated wear can be considered to predict the time-variant damage morphology.	Simulation results were compared to theoretical values.	[108]
Modelling the multi-degradation mechanisms of combined tribocorrosion interacting with static and cyclic loaded surfaces of passive metals exposed to seawater	Model coupling corrosion fatigue (CF) and stress corrosion cracking (SCC) mechanisms. The multi-degradation model is based on surface hardness and corrosion resistance.	Further experiments needed to validate model	[107]

4. Environmental Effects on Tribocorrosion

The influence of tribocorrosion on a diverse set of applications, such as biomedical implants, marine equipment, and machinery components, has been extensively studied. Especially in recent years, research has been further exacerbated by the increasing number of applications and their deployment in harsh environmental conditions. In this section, we will provide an overview of the challenges of tribocorrosion in these applications and discuss the potential of coatings as solutions to mitigate its effects.

4.1. pH (Non-Bio and Marine)

Careful and systematic tests on model and engineering bulk surfaces in different environments show the direction the field should take for coated sample testing, although results show the importance of surface oxide or passive films on the tribocorrosion performance of these bulk materials. Wahl, for example, looked at the tribocorrosion behavior of 2205 duplex stainless steel in 0.6 M NaCl and 0.6 M Na₂SO₄ under reciprocating wear. She found that the presence of aggressive chloride (Cl⁻) ions enhanced material loss at applied anodic potentials within the passive regime for this material. Sliding wear in 0.6 M NaCl increased the amount of material loss by 23%–36% compared to experiments in 0.6 M Na₂SO₄. Wear-induced corrosion was also promoted by the presence of Cl⁻ at 600 and 800 mV_{SCE}, where attack occurred predominately in the ferrite phase and at the ferrite/austenite boundary. Ming Lui studied the tribocorrosion behavior of 304 stainless steel in dilute sulfuric acid and in distilled water using a reciprocating sliding. Damage was caused by micro-cutting and synergism, caused by corrosive embrittlement of the surface layer and damage to the passivation film, causing galvanic corrosion. Liwen Tan reports the tribocorrosion behavior and degradation mechanisms of 316L stainless steel in four industrial corrosion media under potentiostatic control. Unusually, under cathodic protection in NaOH solution, corrosive reactions still occurred, and coupled with wear, led to abnormally high material loss.

Mohsen Feyzi, on the other hand, looked at the tribocorrosion behavior of Ti-6Al-4V alloy and the kinematics of repassivation in buffered saline solution under reciprocating motion between 1 and 15 Hz. Volume loss was maximum at 5 Hz, with a subsequent reduction when increased to 15 Hz. Compared to the total and corrosion losses, mechanical losses showed significant variation with frequency and complex interactions between the normal force and frequency. These findings are contradictory to the general understanding of an increase in the total loss with increasing frequency, i.e., Archard-like behavior. B-B Zhang studied the influence of the solution pH on the tribocorrosion behavior of nickel aluminum bronze (NAB) rubbing against Al₂O₃ using a pin-on-disc tribometer equipped with a potentiostat. The results show that a high pH solution increases corrosion and

gives rise to accelerated material loss. The NAB oxidation process was driven by the dissolution of K_{II} phase at a pH below 4.2, whereas its anodic behavior was dominated by the preferential corrosion attack of copper-rich α -phase within the $\alpha + K_{III}$ eutectoid when the pH was higher than 4.2. The study found that the pure mechanical and corrosion-accelerated wear was due to delamination and abrasive wear processes.

In a related area, Neville addressed the tribochemical phenomena involved in micro-pitting in tribocorrosion systems where different levels of dissolved water are present in a model lubricant [120]. The tribochemical change of the reaction films was studied by X-Ray Photoelectron Spectroscopy (XPS), which confirmed that the (poly)phosphate chain length and tribofilm thickness are reduced with increased dissolved-water levels.

In the literature, studies on tribocorrosion involving NaCl solutions are extensively reported. The effects of nanoscale chemical heterogeneity on the wear, corrosion and tribocorrosion resistance of ZrCuNiAl thin-film metallic glasses were investigated by Wenbo Wang, who found the tribocorrosion resistance of heter-Zr samples to be better than that of homo-Zr samples [121]. Furthermore, examinations of the behavior of uncoated substrates, such as stainless steel, titanium alloys and aluminum alloys, in NaCl solutions yielded consistent results across a range of studies, without presenting any notably unique findings [122–128].

Hesham Mraied showed that alloying aluminum with manganese in a super-saturated solid solution enhances both the wear resistance of aluminum and the protectiveness of its passive layer, thereby significantly improving its overall tribocorrosion resistance in a 0.6M NaCl solution. Higher Mn content increased the ratio of hardness to elastic modulus (H/E) and promoted the formation of a denser and more compact passive film, hence improving the tribocorrosion resistance of Al. In particular, alloying with 20.5 at% Mn led to a 10-fold increase in corrosion resistance and an 8-fold increase in hardness compared to pure Al. Interestingly, the authors developed a simple galvanic cell model to investigate the depassivation–repassivation kinetics during tribocorrosion and found that alloying with 5.2at%Mn led to more than a 10-fold reduction in the current density required to re-passivate similar worn areas generated with pure Al [126].

Kossmann's study [127] assessed the tribocorrosion properties of 316L stainless steel with three industrial surface finishes: passivation (SSO), electropolishing-passivation (SSEP), and micro-undulation (SSM) mechano-chemical, in NaCl solution [129]. The results showed that the SSEP treatment increased chemical wear due to its passive film's properties; the micro-undulated SSM surface decreased contact area and enhanced lubrication, improving tribocorrosion resistance.

Wahl studied the correlation between increasing material loss rates and damage to the protective oxide layer in passivating alloys under tribocorrosion in an electrochemical cell. The findings indicated that sliding mechanical contact under anodic potentials within the passive oxide region led to pitting corrosion and localized increases in electrochemical cell current, particularly in chromium-depleted secondary austenite phases.

Yue Zhang et al. looked at the tribocorrosion behavior of stainless steel 304 in chloride-containing solutions with different alkalinity [130]. They suggest corrosion was accelerated due to the formation of galvanic couples between the mechanical depassivated areas and the surrounding passivated areas. Both the friction coefficient and total material loss decreased with increasing pH, with pure mechanical and corrosion-accelerated wear, including abrasion and delamination, being among the main reasons for material loss. Jingyi Zou looked at 316L stainless steel in 0.1 mol/L NaOH alkaline solution to investigate the synergism between wear and corrosion [131]. Larger material loss was found at a cathodic potential of -0.8 V, and lower material loss at anodic potential, when compared with that under pure wear conditions. The formation of tribo-films with different properties at different potentials was responsible for this performance. The tribo-film formed at -0.8 V had the highest oxygen content and was very brittle. By contrast, the tribo-films formed at anodic potentials were more complete, and the oxygen content was much lower; thus, they were more ductile and could better protect the stainless steel from wear.

Long Xin studied the fretting of Inconel 690TT in NaOH (pH = 9.8) and showed that when normal force increased from 15 to 30 N, fretting was in the gross slip regime (GSR), and wear volume gradually increased [132]. When normal force increased further to 45 N, wear volume significantly decreased due to the fretting changing to the partial slip regime (PSR). Fretting wear broke the passive film at the contacting surface, which caused the worn surface to be more active and prone to corrosion. However, the broken passive film was quickly repaired in subsequent oxidation. The damage and repair of the passive film was found to be strongly dependent on normal force. In GSR, increasing force aggravated the damage, while in PSR, the passive film was not easily damaged.

Junxiao Du studied the tribocorrosion behavior of pure nickel in citrate buffer solution at pH 4.5 [133]. The results show that the wear of nickel was higher in the passive domain due to wear-accelerated corrosion (ΔWc) compared to that in the cathodic domain. Surprisingly, both alumina and zirconia counter-faces were worn by the nickel in the tribocorrosion condition under passive potentials as well as in the dry condition. However, in the cathodic domain, negligible wear was observed on the alumina and zirconia balls. The formation of mixed nickel and aluminum/zirconium oxides was proposed as the wear mechanism of alumina and zirconia.

Espallargas reports on the tribocorrosion of overlay-welded Ni–Cr 625 alloy sliding against alumina in 0.5 M H₂SO₄ and 0.5 M HNO₃ solutions [134]. The tribocorrosion behavior of the alloy in sulfuric acid was found to be similar to that of stainless steels reported in other studies, with much lower wear at cathodic potential compared to passive conditions. However, the behavior in nitric acid was highly influenced by the reduction of nitric acid at the electrode–electrolyte interface. This reaction leads to the oxidation of the alloy even at cathodic potential.

4.2. Biomedical Sectors

The exponential growth of the aging population has resulted in a significant increase in the use of orthopedic prostheses [135] and dental implants [136] to maintain both quality of life and active lifestyles [137]. Tribocorrosion in biomedical applications presents a significant challenge, largely due to the exposure of implants to body fluids and electrolytes at moderate temperatures and to complex, high mechanical stresses [138].

For instance, the environment in the oral cavity is marked high acidity, diverse bacterial interactions, and recurrent mechanical stresses during mastication. In the context of hip and knee joints, the load and frequency of movement can influence wear patterns and the rate of corrosion. Such exposure, in combination with tribocorrosion phenomena that occur when the implant comes into contact with other surfaces such as bone or cartilage [139], can lead to implant failure, tissue damage, inflammation, reduced mobility and pain for patients [16]. Over recent decades, there has been a rise in the incidence of failure and clinical issues associated with prosthetic dental and orthopedic implants [140]. Particularly, dental implant failures are around 1%–20% [141], whereas for orthopedic implants, this number is higher than 35% [142]. Adding to the concern, wear debris with sizes ranging from nanometric to micrometric dimensions can enter the circulatory system and accumulate in cells, lungs and osteoblasts [143].

Metallic biomaterials have played a crucial role in the development of medical implants, which constitute approximately 70%–80% of all implanted materials [144]. The material options are constrained by biocompatibility; the most common biomedical materials include stainless steel, cobalt-based alloys and titanium-based alloys [145]. Each of these materials has unique properties, with some being more suitable for specific applications than others. Stainless steel metal implants, with their high availability and low cost, are commonly used for total hip replacement stems and bone-fixation tools such as nails, screws, and fracture plates [146]. CoCr28Mo6, more commonly known as CoCrMo, has historically been the preferred material in the design of medical implants. However, its use in permanent implants is currently restricted due to the prolonged release of Co, Cr and Ni ions [147]; it should be noted that concerns have been raised about the potential

release of elements (Co, Cr and Ni) from these materials into the body causing allergic reactions in patients [148]. Commercially pure titanium (cpTi) and Ti-6Al-4V are commonly used in bone fusion, bone fixation and joint arthroplasty, both of which give clinical success rates of up to 99% at 10 years [149]. The utilization of titanium in the production of dental implants is largely due to its exceptional biocompatibility, chemical inertness, suitable mechanical properties and outstanding clinical performance, alongside its ability to form a natural protective oxide layer known as TiO₂ [150]. This protective oxide film, ranging from 1.5 to 10 nm in thickness, is credited with providing titanium's excellent corrosion resistance [151]. Nonetheless, there are numerous factors, such as surface friction and scratches incurred during implant placement, which can compromise this protective coating [152]. Furthermore, there is evidence to suggest that concentrations of titanium exceeding 13 ppm can precipitate necrosis in epithelial cells and heighten the vulnerability of peri-implant mucosa epithelial cells to microorganisms [153]. Additionally, the elements vanadium (V) and aluminum (Al) have been implicated in various neurological disorders, including Alzheimer's disease [154].

Therefore, the primary challenge in ensuring the durability and functionality of these biomedical devices is balancing tribocorrosion management with optimal biocompatibility. In response, various research initiatives are developing specialized coatings to improve the structural, tribological and electrochemical properties of these materials to address and mitigate potential health risks. The coated implants currently available on the market are ZrO₂-coated Zr (Smith and Nephew), TiN-coated CoCr or Ti₆Al₄V (Implantcast, Link orthopaedic), TiNbN-coated CoCr (OHST medical technology) and TiN-coated Ti6Al4V (Endotec) [16]. Recent studies on coating techniques for 316L and Ti-6Al-4V alloys have shown promising results in enhancing material properties. Laser cladding of 316L with one to three layers of Fe-based amorphous material resulted in a microstructure evolution from primary FCC to BCC with increasing layers, leading to increased hardness. Notably, a two-layered coating was found to be the most effective [155]. This finding was echoed in another study with 1–12 layers, where again the two-layered coating showed optimal performance [156]. In contrast, arc-spraying of 316L with Fe-based amorphous material demonstrated improved tribocorrosion resistance compared to uncoated 316L SS, particularly during sliding wear in PBS and NaCl solutions [157].

Table 3 provides a summary of various other techniques tested in bio-environments.

4.2.1. Dental

Dental implants, serving as artificial dental roots, are surgically placed into either the upper or lower jawbone, with the advantage of not affecting adjacent healthy teeth. The success rate of these implants is impressive, ranging from 90% to 96.5% [158]. Nevertheless, the increasing demand for dental implants, coupled with the evolving needs of patients, underscores the need for continuous improvement in implant technologies to reduce rejection and replace failed implants [86].

A primary cause of dental implant failure is tribocorrosion, a process that can hasten the deterioration of implant components. This issue is particularly critical in biomedical fields, where implant failures not only impair function but also risk patient health due to the release of harmful wear products. Tribocorrosion is triggered by various factors, including mastication, saliva, pH changes and temperature variations, leading to damage at the implant interfaces [4]. Dental implants are continuously exposed to a moist environment, making them susceptible to corrosion and microbial colonization throughout their lifespan [159].

Specifically, three interfaces in dental implants are prone to fretting corrosion (see Figure 15): the connections between the crown and abutment, the abutment and implant, and the implant and bone. The repetitive loading from biting and chewing can disrupt protective films on these interfaces, accelerating corrosion [160]. This type of damage, caused by micromotion, is known as fretting corrosion [4].

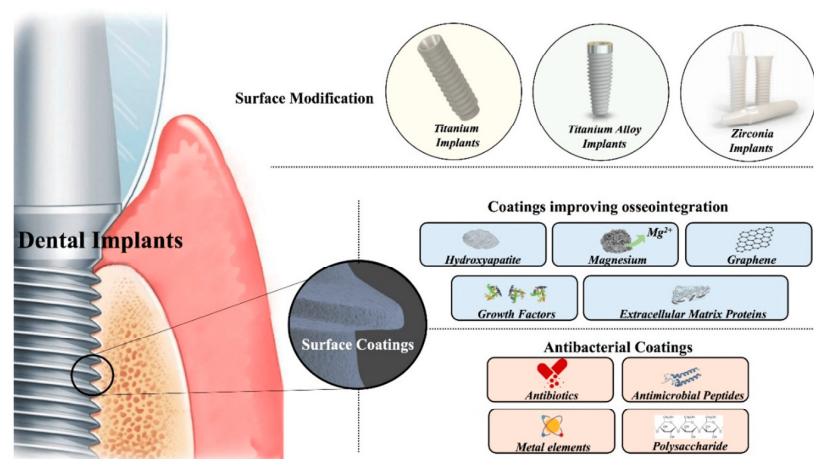


Figure 15. Implants [161].

Coating technology plays a crucial role in enhancing implant performance. Richard et al. investigated coatings of nano-ZrO₂ and Al₂O₃-13 wt% TiO₂ on titanium, finding improved wear and corrosion resistance [162]. One study explored the coating of variously treated titanium substrates with titanium dioxide (TiO₂) films using Low-Pressure Metal Organic Chemical Vapor Deposition (MOCVD), revealing that substrate morphology significantly influences the crystalline structure, wettability, ion release, electrochemical behavior, tribocorrosion performance and nano-mechanical properties of TiO₂ coatings, with sandblasted/acid-etched coated Ti substrates showing the most promising functional properties for dental implant fabrication [163]. Additionally, TiN coatings have gained popularity in dentistry due to their biological properties, such as reducing the release of harmful ions and providing an aesthetic golden color [164].

Alves and co-authors focused on enhancing the tribocorrosion behavior of titanium alloys used in dental implants, particularly from 2013 to 2022. Initial studies on Cp-Ti highlighted the advantages of Plasma Electrolytic Oxidation (PEO) and anodic treatment in enhancing substrate performance through varied surface topographies and compositions [165,166]. Subsequent research expanded to include the anodic treatment of Ti-6Al-4V and cp-Ti surfaces, leading to the development of nanotubular structures and porous designs that significantly improved tribocorrosion resistance [167]. From 2018 to 2021, the effects of electrolyte composition in the Micro-Arc Oxidation (MAO) process on cp-Ti and Ti-6Al-4V were studied. These studies highlighted how the addition of bio-active elements (Ca and P) optimized the tribocorrosion behavior, surface hardness and microstructure [168–171]. For the Ti40Nb alloy, a two-step anodic treatment and heat treatment were employed to develop a TiO₂-based nanotubular surface with improved adhesion, further enhanced by the addition of an extra oxide layer from a fluoride-free electrolyte [172]. Building on that, studies conducted on the Ti-40Nb + TiN and Ti-25Nb-5Fe + TiN alloys revealed that the incorporation of TiN reinforcement, coupled with bio-functionalization, led to substantial improvements in hardness and microstructure as well as the formation of a strongly adhered anatase-rutile TiO₂-based nanotubular layer, significantly boosting both corrosion and tribocorrosion behaviors [173,174]. Apart from the comprehensive studies by Alves, other researchers have also explored the techniques of PEO and MAO on Ti-6Al-4V substrates. For example, Garcia-Cabezón in Spain demonstrated that PEO-Ca/P coatings on these substrates offer enhanced performance due to a higher rutile-to-anatase ratio and smoother surface [175]. Similarly, in China, You Zuo's research indicated that increasing the voltage in MAO coatings adjusts the rutile-to-anatase ratio [176] and incorporating graphene oxide particles notably improves tribocorrosion resistance [177]. Binbin He's study further emphasized the effectiveness of Cu_xO-containing PEO coatings in significantly reducing mass loss [178]. Examples of PEO-treated dental screws are shown in Figure 16.

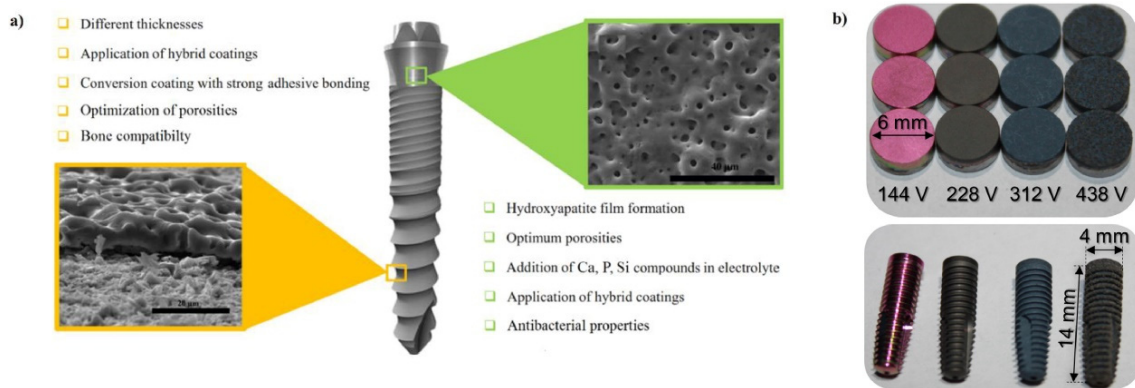


Figure 16. (a) Possible enhancements of titanium implant screws by PEO coating; (b) dental screws coated with PEO in various colors [179].

Among the various coating methods, plasma spray is the predominant technique used clinically for titanium dental implants. Layers of calcium phosphates, primarily consisting of hydroxyapatite ($\text{HA-Ca}_{10}(\text{PO}_4)_6(\text{OH})_2$) are used to coat metallic implants. This composition closely mimics the inorganic portion of bone, thereby facilitating osseointegration. The properties of these coatings, such as porosity and thickness, are critical for facilitating bone cell differentiation [180]. However, the tribocorrosion performance of these coatings is rarely discussed.

4.2.2. Joint Prostheses

A critical issue in the failure of hip implants is wear and corrosion, notably in the metal-on-metal (MoM) design of total hip replacements (THRs), as illustrated in Figure 17. These MoM implants are adversely affected by tribocorrosion, leading to the production of unexpectedly high levels of wear and corrosion debris. This release can cause damage to the bone and tissue surrounding the implant, leading to adverse local tissue reactions (ALTR) or adverse reactions to metal debris (ARMD). The corrosive internal environment of the human body exacerbates tribocorrosion, resulting in the formation of pseudo-tumors around the THR area due to increased wear particles [181]. Additionally, the increased tribocorrosion reaction in these implants leads to a higher release of metal ions, which can potentially lead to tumor formation in various body regions, as these ions are transported through the bloodstream [182]. Reactions such as pain, implant loosening, and device failure, as well as the subsequent need for revision surgery, which requires the removal and replacement of faulty implants, have been observed. These issues have prompted responses from healthcare authorities such as the Food and Drug Administration (FDA) [183].

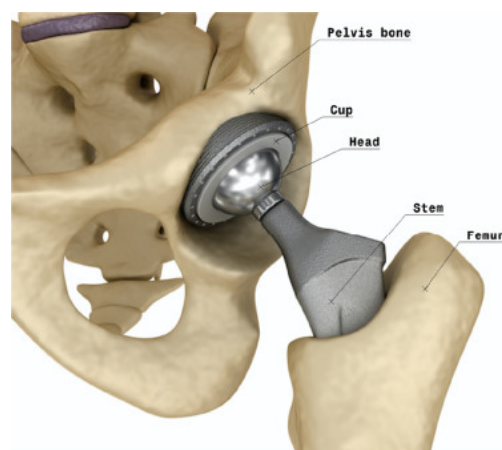


Figure 17. Total hip arthroplasty [184].

The recent literature has documented the occurrence of mixed forms of damage on retrieved hip implants, including wear, corrosion and fretting corrosion [4]. This damage is primarily observed in two critical areas: the sliding corrosion at the femoral head and acetabulum bearings, and the fretting corrosion at the taper junction connecting the femoral head to the stem [185]. Clinically, the modular junction between the hip implant's neck and head is susceptible to micromotions, typically in the range of 5–15 μm , as cited in studies [186,187]. These micromotions within the corrosive biological environment can induce fretting corrosion, potentially leading to implant loosening and the formation of harmful degradation products [4]. Current research efforts are predominantly focused on coatings applied on bearing surfaces to reduce wear and corrosion, particularly for solving the sliding corrosion problems.

Regarding titanium nitride-coated hip implants, Harman et al. [188] and Raimondi and Pietrabissa [189] documented the failure of these implants when paired with UHMWPE liners. Their respective studies revealed significant degradation in the coatings of implants retrieved after short usage periods. Specifically, Harman et al. identified delamination and adhesive wear, whereas Raimondi and Pietrabissa observed a saw-toothed degradation pattern and heightened surface roughness on the coatings, factors that were associated with increased material loss from the UHMWPE liners.

It is important to recognize that the wear behavior in human hip joint differs significantly from the reciprocating sliding wear seen in hip simulators, incorporating diverse motion paths, resting periods and strokes. The risk of sudden fractures, especially with the brittle nature of ceramic materials, is a significant concern. There have been unsuccessful introductions to the market, such as DLC-coated implants. This was reflected in a clinical study by Taeger et al., which specifically compared the performance of DLC coatings on CoCrMo femoral heads with alumina-oxide ceramic heads. Their follow-up investigation revealed a significant disparity, with DLC-coated implants exhibiting considerably lower survival rates than their alumina counterparts, mainly due to mechanical failures, particularly delamination of the coating [190]. In the quest for an ideal coating for medical implants, ongoing advancements and emerging technologies are bringing this goal within reach. The significant amount of research in progress offers hope for the future clinical implementation of various effective combination coatings, likely to significantly improve patient outcomes [142].

Coating technology remains a valuable method for enhancing resistance against tribocorrosion, with the caveat that issues such as delamination need to be resolved, and the gap between in vitro and in vivo study results needs to be narrowed [4]. Moreover, there is increasing interest in adapting these advanced coating technologies to other applications, like hip modular-tapers, where fretting-corrosion processes are predominant.

Table 3. Overview of coating techniques applied on different alloys to enhance tribocorrosion resistance.

Substrate	Tech	Solution	Test	Findings	Ref.
Ti-6Al-4V	Thermal sprayed Alumina, Alumina-Zirconia, Alumina-titania	bovine calf serum (BCS)	OCP	The ceramic coatings primarily suffered from mechanical wear rather than corrosion. The nanostructured bilayered IDZAT coating demonstrated the best performance.	[191]
316L	Dipping polyurethane (PU)–polydimethylsiloxane (PDMS) blended coatings	Ringer's solution	OCP	The wear volume and the friction coefficient of PU–PDMS coatings decreased with the increased PU concentration in the blend. Polymer-coated samples containing up to 50% PDMS prevented corrosive wear. The PU25–PDMS75 coating could not protect the surface due to its weaker mechanical properties.	[192]
304	Electrodeposition Co/nano-CeO ₂	Hank's solution	EIS	The inclusion of nano-CeO ₂ particles into the cobalt matrix by electroco-deposition significantly reduces the friction coefficient, wear weight loss and corrosion damage.	[193]

Table 3. Cont.

Substrate	Tech	Solution	Test	Findings	Ref.
304	PVD calcium phosphate-calcium titanate	Hank's solution	Polarization OCP	Fretting: Calcium titanate coatings showed reduced wear of the bone compared to bare stainless steel, with wear decreasing as the calcium titanate content increased. Calcium titanate coatings are potentially more effective candidate materials than calcium phosphate coatings for bone tissue replacement in hip prostheses.	[194]
Ti-6Al-4V (additive manufactured)	PVD TiN	25%(v/v) newborn bovine serum (17 g/L total protein content) diluted by PBS	OCP	Duplex-TiN coatings were applied on both ALM and traditionally wrought manufactured Ti-6Al-4V substrates. The coatings enhanced hardness (from 3.5 GPa to 14–15 GPa), improved corrosion resistance and showcased excellent wear resistance (wear depth of 0.3 µm against a coating thickness of 3–6 µm). The coated materials displayed the ability to rapidly recover their protective layer after wear tests.	[195]
Ti	plasma spraying Ti-6Al-4V-TiB-TiN	Hank's solution	PDP OCP	The tests also revealed domination of synergistic effects, i.e., corrosion affects wear more than wear affects corrosion. Increasing the deposition speed and/or decreasing the plasma power led to an increase in mechanical wear and corrosion loss.	[196]
Ti	double-glow plasma alloying Nb	Ringer's solution	OCP	DG-Nb wear rate is merely 4.92% of that of Pure Ti.	[197]
Ti, Ti-6Al-4V, Ti13Nb13Zr	CVDNanocrystalline diamond (NCD) coatings	9 g/L NaCl	OCP	NCD coatings showed promise in corrosion resistance; their response under combined wear and corrosion was mixed. Notably, the occurrence of blistering could hinder the long-term performance of such implants.	[198]

4.3. Marine and Offshore Sector

Marine equipment faces distinct tribocorrosion challenges, greatly impacted by an environment characterized by high salinity, low electrical resistivity and continuous mechanical stress. These conditions adversely affect a range of materials, including stainless steel and marine-grade alloys. The situation is exacerbated by the sector's growth, driven by global efforts to reduce greenhouse gas emissions. The expansion of offshore energy production, encompassing sectors such as oil and gas platforms, deep-sea mining operations, thermal recovery systems, wind turbines, wave/tidal energy systems and mooring line installations, intensifies the tribocorrosion challenges faced in these demanding marine environments. In response to these challenges, there is a concerted effort among governments, industry experts and researchers. This collaboration focuses on developing new materials, coatings and monitoring techniques that are robust enough to endure the demanding conditions of the offshore environment [199,200]. To mitigate these effects and protect these structures, standards like ISO 12944 and NORSOK M-501 are utilized [201,202]. They help categorize the corrosivity of offshore installations with classifications like C5-M and Im2 (see Table 4), guiding the implementation of appropriate protective measures [203].

Table 4. Typical coating systems employed in offshore applications in the different exposure zones with the desired properties and corrosivity category (ISO 12944) [203].

Exposure Zone	Category (ISO 12944)	Coating System	Desirable Coating Properties
Atmospheric	C5-M	Zinc-rich epoxy primer (60–100 μm) Epoxy intermediate layer (100–120 μm) Polyurethane topcoat (50–80 μm)	Corrosion-resistant, Erosion-resistant, anti-icing, UV-resistant
Splash and tidal	C-M and Im2	Two or three epoxy-based coats (>1000 μm in total) Polyurethane topcoat (50–80 μm)	Combination of atmospheric and submerged coatings' properties
Submerged	Im2	Two or three epoxy-based coats (>450 μm in total)	Corrosion-resistant, antifouling, wear-resistant

In managing tribocorrosion, the marine and offshore industries must strategically select coating systems based on the environmental conditions specific to each exposure zone [204]. Referring to Figure 18, structures within the atmospheric zone require coatings that deliver resistance to corrosive elements and additional protection against UV radiation and icing, as indicated by the ISO 12944 C5-M category. In the splash and tidal zones, where structures are intermittently exposed to both air and seawater, the coatings must embody a combination of atmospheric and submerged coatings' properties. For fully submerged structures, the focus shifts primarily to corrosion resistance, while also incorporating antifouling and wear-resistant characteristics as necessitated by the Im2 category [203].

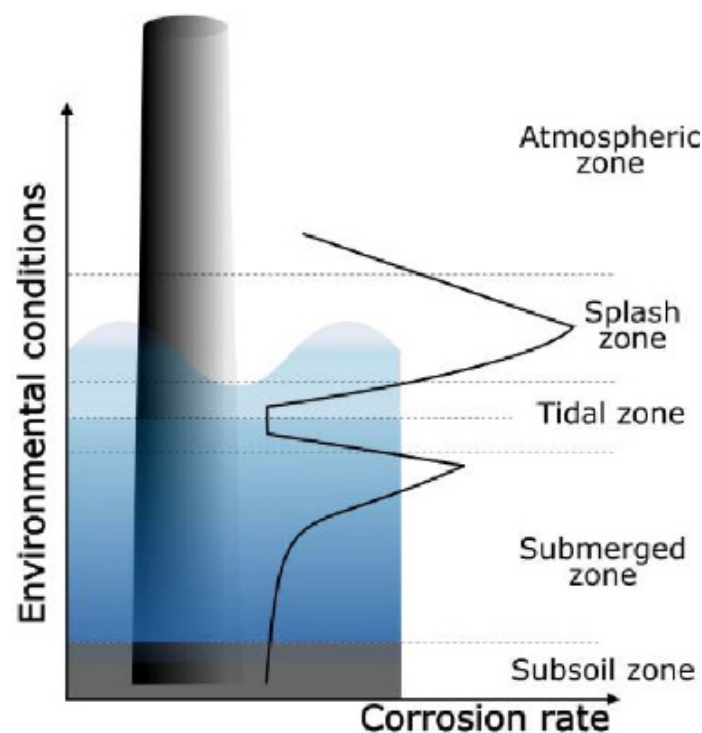


Figure 18. Corrosion rate [203].

Steel remains a pivotal structural material in offshore settings. To safeguard these structures against harsh marine environments, significant advancements in protective coatings have been made. Aiyang Wang's team studied the effectiveness of various PVD coatings, such as Cr/GLC- and DLC-based variants, in a 3.5 wt% NaCl environment. Their studies highlighted that while some coatings like TiC_x/DLC excel in short-term durability due to high hardness, others like Ti-TiC_x/DLC offer superior long-term performance through a balance of hardness and toughness [205–207]. Studies by other researchers have

demonstrated that PVD coatings exhibit diverse performances under both stationary and dynamic conditions. These studies highlight that certain coatings provide enhanced resistance to wear and corrosion, showcasing the range of effectiveness these coatings can offer in different environmental scenarios [208–212]. The effectiveness of these coatings is also influenced by the substrate material, as seen in studies involving different steel types with PVD CrCN coatings [213]. Additionally, coatings like CrN and Cr/CrCN on steel have been observed to alter wear mechanisms depending on environmental conditions, highlighting the importance of coating composition [214,215]. Innovations in coatings such as Ti, TiSiC, TiSiCN, AlFeCrNiMo and W-doped DLC have been shown to improve wear resistance and durability [216,217]. Moreover, nanocomposite structures like TiSiN-Cu and CrN/AlN coatings provide enhanced mechanical properties and resistance, proving beneficial in corrosive environments [218,219]. Moreover, plasma nitriding before PVD coating can significantly enhance the corrosion and tribocorrosion resistance of steels, making them suitable for marine applications [220]. In addition to PVD, there have been significant advancements in Thermally Sprayed Aluminum (TSA) coatings, which have markedly enhanced their capability to protect steel structures in offshore environments. Composite coatings of TSA with Al₂O₃ particles have lower wear rates and friction coefficients than pure Al coatings [221]. The integration of the Plasma Electrolytic Oxidation (PEO) technique into TSA coatings has led to the development of a robust TSA/PEO duplex coating. Extensively tested for sliding wear, electrochemical corrosion, and tribocorrosion in synthetic seawater, it shows enhanced durability and resistance in harsh marine environments [222]. Ceramic materials are traditionally favored for their wear and corrosion resistance but are limited by brittleness. This has led to the innovation of Ti-C-N coatings, which balance hardness with toughness, addressing the brittleness issue [223]. Complementing these, metal-ceramic coatings applied via High-Velocity Oxygen Fuel (HVOF) spraying techniques are particularly effective for deep-sea equipment, where conventional oil lubrication is insufficient. Coatings such as WC-based variants offer high hardness and wear resistance, effectively tackling the multifaceted tribocorrosion challenges in marine settings [224]. Further details on other studies are provided in Table 5.

Titanium, often termed “Ocean Metal”, is renowned for its light weight, high strength and exceptional corrosion resistance, particularly against saltwater and marine atmospheric conditions. This makes it an ideal material for marine engineering, marking it as a pivotal material in this field. Kuptsov deposited TiC/C coatings on Ti substrate using electro-spark deposition (ESD). By altering electrode polarity and pulse energy, control over the carbon content, microstructure and phase composition of the modified Ti layer was achieved. The results show coatings with an upper graphite layer exhibited low friction and high corrosion resistance in saltwater [225]. Recent research towards coatings for titanium alloy substrates, particularly Ti-6Al-4V, has solidified its status as one of the key materials in marine engineering, being especially suitable for light marine equipment. Extensive research on PVD CrMoSiCN and CrMoSiN coatings for Ti-6Al-4V alloys was conducted by Zhou. The author discovered that these coatings exhibited varying tribocorrosion behaviors, which were influenced by the Ag target current. The study revealed that with an increase in the Ag current, the tribocorrosion mechanisms of CrMoSiCN/Ag coatings shifted, highlighting different wear resistance levels under varying conditions [226–229]. Different PVD coatings like TiAlCN and TiSiN/Ag were studied by Li, including nitrided TiSiCN. This research demonstrated that annealing could enhance the corrosion resistance and reduce the friction of TiSiN and TiSiN/Ag coatings. The studies also revealed that the carbon content in the TiSiCN coating significantly influenced its tribocorrosion properties, with its nanocomposite structure and graphitization effects playing a crucial role in wear reduction [230–235].

The exploration of advanced coating technologies in the marine sector is a pivotal response to its unique tribocorrosion challenges, reflecting the evolving needs and dynamic solutions being developed. This comprehensive review highlights the industry’s commitment to enhancing the durability and performance of marine structures and ma-

chinery, from adopting robust coatings like Thermally Sprayed Aluminum (TSA) to using innovative materials like titanium alloys. The strategic selection of these coatings, tailored to specific environmental exposures and operational requirements, is crucial for both static and dynamic marine components. Static components, such as hull plates, deck structures and anchoring systems, require coatings with strong anti-corrosive properties and enhanced wear resistance due to their continuous exposure to seawater and marine sediments. Conversely, dynamic components like propeller blades, rudder hinges and winches necessitate coatings that not only resist wear and corrosion but also reduce friction to maintain operational efficiency. This specialized approach, driven by ongoing research and collaborative efforts across academia and industry, is vital for ensuring the functionality and longevity of marine machinery. It embodies a dedicated strategy to overcome the multifaceted challenges of marine engineering, ensuring that structures and equipment can withstand the harsh marine environment while fostering sustainable and efficient offshore operations.

Table 5. Overview of coating techniques used on marine equipment for tribocorrosion resistance.

Substrate	Tech	Interlayer	Solution	Tests	Findings	Ref.
AISI 1045	PVD Cr/CrN	Nitrided	3.5 wt% NaCl	OCP, PDP	A clear synergy effect of over 30% between friction and corrosion; the synergy effect is caused by the fact that corrosion processes create local cavities which, at successive time intervals, are most likely to intensify mechanical wear. The area around the cavities facilitates plastic deformation, the initiation of cracking of cyclically deformed layers and the tearing off of larger fragments of material (especially at higher unit pressures in the frictional contact zones).	[236]
316L, TC4, and H65 copper	PVD Si-Doped TiSiN-Ag		artificial seawater	OCP, PDP	TiSiN-Ag composite coatings with 8 wt.% Si doping exhibit superior characteristics. These coatings' network structure effectively hinders the generation and growth of cracks. Si doping content can help mitigate the presence of defects such as pinholes and cracks.	[237]
Ti-6Al-4V	W-DLC CrN + a-C:H:W HVOF Cr ₃ C ₂ in Ni/Cr Ion implantation nitriding		artificial seawater	OCP, PDP	The ion implantation treatment on Ti6Al4V substrate yielded the best static corrosion resistance. The W-DLC-coated Ti6Al4V substrate exhibited the most stable and lowest friction, leading to a commendable wear and corrosion resistance in artificial seawater. Both the HVOF coating- and ion implantation-treated substrates had noticeable crack initiation, increasing susceptibility to localized corrosion.	[238]
F22 steel	Thermal spray Fe-based amorphous		artificial seawater	OCP, PDP	Synergy effect: Wear-induced material loss (<i>W</i>) is the major material damage under the current experimental conditions. Seawater aided in lubrication and reducing friction.	[239]

Table 5. Cont.

Substrate	Tech	Interlayer	Solution	Tests	Findings	Ref.
SS316	Thermal spray WC/Ni60		artificial seawater		The WC phases in the coating help resist wear, while the Ni-based materials improve corrosion resistance.	[240]
SS316	Laser cladding titanium carbonitride		3 M NaCl saturated solution	OCP, PDP	316L laser claddings reinforced with titanium carbonitride grains improved tribocorrosion performance by over 10-fold in certain conditions. The optimized addition of (Ti,Mo)(C,N)-Ni powder led to homogeneously distributed reinforcements, enhancing durability. Inappropriate quantities of (Ti,Mo)(C,N)-Ni powder can cause either high agglomerations or uneven dispersion.	[241]
SS304	High-Intensity Pulsed Ion Beam (HIPIB) CrN/TiN		3.5 wt% NaCl	OCP	Coated surfaces present excellent tribocorrosion properties in seawater, showcasing a high open circuit potential, low coefficient of friction and low specific tribocorrosion rate, all without pitting corrosion due to the high surface integrity, stable interfaces and dense microstructure.	[242]
R4 mooring chain	pack cementation method FeAl		3.5 wt% NaCl	OCP, PDP	Improved corrosion resistance was offered by the aluminized coating, with the oxide layer on the surface playing a key role in this improvement. However, its wear resistance decreased due to the presence of brittle phases.	[243]

5. Conclusions and Future Challenges

Surface design often must consider wear, friction and corrosion rates, which often have antagonistic relationships and involve complicated interactions between multiple mechanisms at different scale lengths within tribocorrosion contacts. However, the tribologically induced stresses can create damage propagation and accelerate corrosion either within the coating or at the coating–substrate interface. Any crack systems in the coating or porosity allow the environment to permeate into the coating and eventually to the coating/substrate interface, accelerating substrate corrosion and coating disbondment and often causing early failure or poor performance.

This review has highlighted the role of stress as a driver for damage processes and the need to understand the stress fields induced under sliding or rolling contacts. Stress and dynamic loadings are shown to enhance both wear and corrosion and, therefore, tribocorrosion. The environment (pH and temperature) is also shown to have a strong influence on tribocorrosion performance. Experiments should monitor and report on the key factors listed in Figure 1 (surface film, recovery, composition, environment, friction and wear, microstructural changes both on the surface and subsurface, roughness changes, occurrence of electrochemical reaction(s) and so on). This would allow a more generic understanding across the very diverse set of coatings and surface modification techniques being investigated.

Coating solutions being developed for tribocorrosion applications include a whole range of Ni-based electrodeposited coatings, hard and tough coatings and high impedance

coatings such as PECVD N and Si-doped diamond. Hybrid and multilayered coatings are also being used to control damage penetration into the coating (to increase toughness) and to manage stresses. A particular focus involves the combination of various treatment techniques. For example, the use of surface treatment methods such as Plasma Electrolytic Oxidation (PEO) alongside deposition techniques is gaining momentum.

In biomedical applications, the development and utilization of coated implants have gained significant traction. The market currently offers a diverse range of these implants, featuring advanced coatings such as Titanium Nitride (TiN), Titanium Niobium Nitride (TiNbN), Zirconium Nitride (ZrN) and surface-treated Zirconium, which results in an oxidized surface layer (ZrO_x). Additionally, a wide array of candidate materials is under active research, including carbon-based, silicon nitride and chromium nitride, as well as Titanium-based (Ti-based), Zirconium-based (Zr-based), Tantalum-based (Ta-based), and alumina-based coatings. However, a notable discrepancy is seen between the outcomes of simulator tests and actual in vivo (clinical) usage of these coatings. In several instances, coatings that have successfully passed rigorous laboratory testing have failed to demonstrate similar performance in clinical settings. A case in point is the introduction and subsequent market withdrawal of Diamond-Like Carbon (DLC)-coated implants. Such instances raise serious concerns, as the failure of coatings within the body can lead to severe complications. This situation highlights the urgent need for more reliable and realistic testing methods.

Global interest in marine research is increasing, with recent notable contributions from a diverse set of countries, including China. In this field, thermal spray techniques have become particularly valuable. For example, aluminum coatings are being used on submerged components and often post-deposition treated with an organic sealant. Additionally, Thermally Sprayed Carbide Coatings, known for their high hardness and wear resistance, are widely employed, offering enhanced corrosion resistance. Research in this area frequently adopts a trial-and-error methodology, adapting techniques from other applications. Recent advances have also seen the use of thin-film techniques, such as Diamond-Like Carbon (DLC) and Nitride coatings, applied via Physical Vapor Deposition (PVD). However, it remains crucial to recognize the distinct and challenging nature of the marine environment in these applications for thin-film technologies.

The review has also shown the importance of the microstructure, the active phases that are dissolved and the role of surface films and their composition (oxide or passive) in tribocorrosion performance which, although discovered for bulk materials, is equally applicable to coating performance. New techniques reveal the response of surfaces to tribocorrosion (i.e., scanning electrochemical microscopy).

Modelling tribocorrosion has yet to embrace the full range of coatings and the fact that some coatings/environments result in reduced wear and thus are antagonistic rather than synergistic. The actual synergistic/antagonistic mechanisms are not well understood, making tribocorrosion difficult to model. These interactions need to be fully understood to enable modelling to advance. Other areas that need to be included are the role of debris in the contact, temperature/flash temperature, areal roughness evolution, the chemistry of oxides and corrosion reactions, complete and partial film removal and growth rates, porosity and defects, microstructural and compositional evolution, selective phase corrosion attack, environmental changes in the interface, strain hardening/phase transformations, material transfer between mating surfaces, the porosity of coating and subsequent permeation of electrolytes to the coating–substrate interface, interfacial corrosion/cathodic disbondment, galvanic coating–substrate interactions, the role of corrosion products and intrinsic residual and surface stresses. Also, repassivation or oxidation rates are often unknown, hampering prediction of tribocorrosion, and the Archard is often applied without evidence that Archard is applicable.

A significant challenge in the field is the lack of overarching design principles. The application of coating processes is quite varied, making it challenging to form a general understanding. The diversity in testing methods as well as the assessment and characteri-

zation of the tribocorrosion components and mechanisms makes it difficult to compare the performance of different coatings and therefore coating selection. The diversity in coating types and compositions further complicates the development of a generic understanding. An often-overlooked aspect is the cost–benefit analysis to facilitate the transition of scientific research into practical industrial applications, which also hinders the uptake of research outcomes into businesses.

Moreover, several factors still require thorough investigation, such as the effects of cyclic-loading stress. There is also a need to ensure that coatings developed in laboratories are effective when used in service. Variability in coatings from different production batches poses a challenge; thus, addressing issues of repeatability and reproducibility is critical for consistent quality assurance in coating applications.

Funding: This research received no external funding.

Conflicts of Interest: The authors declare no conflict of interest.

Abbreviation

a-C	Amorphous carbon
ALTR	adverse local tissue reactions
AP	aluminum phosphate
ARMD	adverse reactions to metal debris
CBPCC	chemically bonded phosphate ceramic coating
CF	corrosion fatigue
CVD	Chemical Vapor Deposition
DLC	Diamond-Like Carbon
EIS	Electrochemical Impedance Spectroscopy
ESD	electro-spark deposition
FDA	Food and Drug Administration
GSR	gross slip regime
H/E	hardness to elastic modulus
HA	hydroxyapatite
HEA	High-entropy alloy
HVOF	High-Velocity Oxygen Fuel
IBAD	Ion Beam-Assisted Deposition
MAO	Micro-Arc Oxidation
MOCVD	Metal Organic Chemical Vapor Deposition
MoM	metal-on-metal
NAB	nickel aluminum bronze
OCP	open circuit potential
PAE	pulsed arc evaporation
PDMS	polydimethylsiloxane
PDP	Potentiodynamic Polarization
PECVD	plasma-enhanced chemical vapor deposition
PEO	Plasma Electrolytic Oxidation
PU	polyurethane
PVP	polyurethane and polyvinylpyrrolidone
PWRs	Pressurized Water Reactors
SCC	stress corrosion cracking
THR	total hip replacement
TO	Thermal Oxidation
TSA	Thermally Sprayed Aluminum
UCFT	ultrasonic cold forging technology
UHMWPE	Ultra-High Molecular Weight Polyethylene
UNSM	Ultrasonic nanocrystal surface modification
XPS	X-Ray Photoelectron Spectroscopy

References

1. Kumar, V.; Agarwal, A.K.; Jena, A.; Upadhyay, R.K. (Eds.) *Advances in Engine Tribology*; Springer: Singapore, 2022; ISBN 9789811683367.
2. López-Ortega, A.; Arana, J.L.; Bayón, R. Tribocorrosion of Passive Materials: A Review on Test Procedures and Standards. *Int. J. Corros.* **2018**, *2018*, 7345346. [[CrossRef](#)]
3. Blau, P.J.; Wood, R.; Stack, M.M.; Mischler, S.; Jiang, J.; Drees, D.; Rocha, L.A.; Wimmer, M.A.; Celis, J.-P.; Cowan, R. Future Needs and Challenges in Tribo-Corrosion Research and Testing. In *Tribo-Corrosion: Research, Testing, and Applications*; Blau, P.J., Celis, J.-P., Drees, D., Eds.; ASTM International: West Conshohocken, PA, USA, 2013; pp. 214–226, ISBN 978-0-8031-7549-5.
4. Mathew, M.T.; Cheng, K.; Sun, Y.; Barao, V.A.R. The Progress in Tribocorrosion Research (2010–2021): Focused on the Orthopedics and Dental Implants. *J. Bio-Tribo-Corros.* **2023**, *9*, 48. [[CrossRef](#)]
5. Oluwatosin Abegunde, O.; Titilayo Akinlabi, E.; Philip Oladipo, O.; Akinlabi, S.; Uchenna Ude, A. Overview of thin film deposition techniques. *AIMS Mater. Sci.* **2019**, *6*, 174–199. [[CrossRef](#)]
6. Pinto, G.; Silva, F.; Porteiro, J.; Mínguez, J.; Baptista, A. Numerical Simulation Applied to PVD Reactors: An Overview. *Coatings* **2018**, *8*, 410. [[CrossRef](#)]
7. Bozkurt, Y.; Kovaci, H.; Yetim, A.; Celik, A. Tribocorrosion properties and mechanism of a shot peened AISI 4140 low-alloy steel. *Surf. Coat. Technol.* **2022**, *440*, 128444. [[CrossRef](#)]
8. Liu, R.; Yuan, S.; Lin, N.; Zeng, Q.; Wang, Z.; Wu, Y. Application of ultrasonic nanocrystal surface modification (UNSM) technique for surface strengthening of titanium and titanium alloys: A mini review. *J. Mater. Res. Technol.* **2021**, *11*, 351–377. [[CrossRef](#)]
9. Wood, R.J.K. Tribo-corrosion of coatings: A review. *J. Phys. Appl. Phys.* **2007**, *40*, 5502–5521. [[CrossRef](#)]
10. Zeisel, H.; Durst, F. *Computations of Erosion–Corrosion Processes in Separated Two-Phase Flows NACE Corrosion*; NACE: Phoenix, AZ, USA, 1990.
11. Vignal, V.; Mary, N.; Ponthiaux, P.; Wenger, F. Influence of friction on the local mechanical and electrochemical behaviour of duplex stainless steels. *Wear* **2006**, *261*, 947–953. [[CrossRef](#)]
12. Zhou, S.; Stack, M.M.; Newman, R.C. Characterization of synergistic effects between erosion and corrosion in an aqueous environment using electrochemical techniques. *Corrosion* **1996**, *52*, 934–946. [[CrossRef](#)]
13. Matsumura, M. Erosion-corrosion of metallic materials in slurries. *Corros. Rev.* **1994**, *12*, 321–340. [[CrossRef](#)]
14. Neville, A.; Hodgkiess, T.; Xu, H. An electrochemical and microstructural assessment of erosion–corrosion of cast iron. *Wear* **1999**, *233*, 523–534. [[CrossRef](#)]
15. Mathew, M.T.; Srinivasa Pai, P.; Pourzal, R.; Fischer, A.; Wimmer, M.A. Significance of Tribocorrosion in Biomedical Applications: Overview and Current Status. *Adv. Tribol.* **2009**, *2009*, 250986. [[CrossRef](#)]
16. Skjöldebrand, C.; Tipper, J.L.; Hatto, P.; Bryant, M.; Hall, R.M.; Persson, C. Current status and future potential of wear-resistant coatings and articulating surfaces for hip and knee implants. *Mater. Today Bio* **2022**, *15*, 100270. [[CrossRef](#)] [[PubMed](#)]
17. Puthillam, U.; Selvam, R.E. Tribocorrosion in biomaterials and control techniques: A review. *Corros. Rev.* **2023**. [[CrossRef](#)]
18. Wood, R.J.K. Marine wear and tribocorrosion. *Wear* **2017**, *376–377*, 893–910. [[CrossRef](#)]
19. Wood, R.J.K. Erosion–corrosion interactions and their effect on marine and offshore materials. *Wear* **2006**, *261*, 1012–1023. [[CrossRef](#)]
20. Monticelli, C.; Balbo, A.; Zucchi, F. Corrosion and tribocorrosion behaviour of thermally sprayed ceramic coatings on steel. *Surf. Coat. Technol.* **2011**, *205*, 3683–3691. [[CrossRef](#)]
21. Monticelli, C.; Balbo, A.; Zucchi, F. Corrosion and tribocorrosion behaviour of cermet and cermet/nanoscale multilayer CrN/NbN coatings. *Surf. Coat. Technol.* **2010**, *204*, 1452–1460. [[CrossRef](#)]
22. Ge, Y.; Cheng, J.; Yan, C.; Xue, L.; Zhang, B.; Liang, X. Devitrification and sliding wear behaviors of AlFeSi metallic glass coatings. *J. Mater. Res. Technol.* **2021**, *15*, 7022–7032. [[CrossRef](#)]
23. Cao, L.; Liu, J.; Wan, Y.; Pu, J. Corrosion and tribocorrosion behavior of W doped DLC coating in artificial seawater. *Diam. Relat. Mater.* **2020**, *109*, 108019. [[CrossRef](#)]
24. Shen, Y.; Luo, J.; Liao, B.; Zhang, X.; Zhao, Y.; Zeng, X.; Chen, L.; Pang, P.; Bao, F. Tribocorrosion and tribological behavior of Ti-DLC coatings deposited by filtered cathodic vacuum arc. *Diam. Relat. Mater.* **2022**, *125*, 108985. [[CrossRef](#)]
25. Yasir, M.; Zhang, C.; Wang, W.; Xu, P.; Liu, L. Wear behaviors of Fe-based amorphous composite coatings reinforced by Al₂O₃ particles in air and in NaCl solution. *Mater. Des.* **2015**, *88*, 207–213. [[CrossRef](#)]
26. Kuptsov, K.A.; Sheveyko, A.N.; Manakova, O.S.; Sidorenko, D.A.; Shtansky, D.V. Comparative investigation of single-layer and multilayer Nb-doped TiC coatings deposited by pulsed vacuum deposition techniques. *Surf. Coat. Technol.* **2020**, *385*, 125422. [[CrossRef](#)]
27. Hu, K.; Liu, X.; Zhang, S.; Xue, Z.; Yang, Y.; Yang, K. Tribocorrosion behavior of HVOF sprayed WC-based cermet coatings in sodium chloride solution environment in relation to binder phases. *Surf. Coat. Technol.* **2022**, *435*, 128248. [[CrossRef](#)]
28. Pileggi, R.; Tului, M.; Stocchi, D.; Lionetti, S. Tribo-corrosion behaviour of chromium carbide based coatings deposited by HVOF. *Surf. Coat. Technol.* **2015**, *268*, 247–251. [[CrossRef](#)]
29. Rodrigues, I.; Nunes, B.; Almeida, A.; Vilar, R.; Figueiredo-Pina, C.G. Are Cr₃C₂-25(80Ni₂₀Cr) coatings deposited by HVOF suitable for reciprocating sliding contacts under aqueous media? *Tribol. Int.* **2020**, *149*, 105825. [[CrossRef](#)]
30. Caha, I.; Alves, A.; Affonco, L.; Lisboa, P.; da Silva, J.; Rocha, L.; Pinto, A.; Toptan, F. Corrosion and tribocorrosion behaviour of titanium nitride thin films grown on titanium under different deposition times. *Surf. Coat. Technol.* **2019**, *374*, 878–888. [[CrossRef](#)]

31. Merl, D.; Panjan, P.; Cekada, M.; Gselman, P.; Paskvale, S. Tribocorrosion degradation of protective coatings on stainless steel. *Mater. Tehnol.* **2013**, *47*, 435–439.
32. Cui, W.; Niu, F.; Tan, Y.; Qin, G. Microstructure and tribocorrosion performance of nanocrystalline TiN graded coating on biomedical titanium alloy. *Trans. Nonferrous Met. Soc. China* **2019**, *29*, 1026–1035. [[CrossRef](#)]
33. Cui, W.; Cheng, J.; Liu, Z. Bio-tribocorrosion behavior of a nanocrystalline TiZrN coating on biomedical titanium alloy. *Surf. Coat. Technol.* **2019**, *369*, 79–86. [[CrossRef](#)]
34. Sáenz de Viteri, V.; Barandika, G.; Bayón, R.; Fernández, X.; Ciarsolo, I.; Igartua, A.; Pérez Tanoira, R.; Moreno, J.E.; Peremarch, C.P.-J. Development of Ti–C–N coatings with improved tribological behavior and antibacterial properties. *J. Mech. Behav. Biomed. Mater.* **2016**, *55*, 75–86. [[CrossRef](#)]
35. Tijerina-Gonzalez, J.L.; Hernandez-Rodriguez, M.A.L.; Lozano, D.E.; Martinez-Cazares, G.M.; Bedolla-Gil, Y. Tribological Characterization of AlCrN, AlTiN, AlTiON, and AlCrON Coatings on CoCrMo Alloy. *Tribol. Trans.* **2021**, *64*, 119–125. [[CrossRef](#)]
36. Pana, I.; Vladescu, A.; Constantin, L.; Sandu, I.; Dinu, M.; Cotrut, C. In Vitro Corrosion and Tribocorrosion Performance of Biocompatible Carbide Coatings. *Coatings* **2020**, *10*, 654. [[CrossRef](#)]
37. de Oliveira, S.M.M.; da Silva, N.S.; Sene, A.; Gandra, R.F.; Junges, D.S.B.; Ramos, M.A.R.; Vieira, L. Comparative Study of *Candida albicans* Inactivation by Nonthermal Plasma on Stainless Steel with and without Diamond-like Carbon Film. *ACS Omega* **2019**, *4*, 6891–6902. [[CrossRef](#)]
38. Bayon, R.; Igartua, A.; Gonzalez, J.; de Gopegui, U. Influence of the carbon content on the corrosion and tribocorrosion performance of Ti-DLC coatings for biomedical alloys. *Tribol. Int.* **2015**, *88*, 115–125. [[CrossRef](#)]
39. Liu, J.; Wang, X.; Wu, B.; Zhang, T.; Leng, Y.; Huang, N. Tribocorrosion behavior of DLC-coated CoCrMo alloy in simulated biological environment. *Vacuum* **2013**, *92*, 39–43. [[CrossRef](#)]
40. Azzi, M.; Paquette, M.; Szpunar, J.; Klemberg-Sapieha, J.; Martinu, L. Tribocorrosion behaviour of DLC-coated 316L stainless steel. *Wear* **2009**, *267*, 860–866. [[CrossRef](#)]
41. Oliveira, S.M.M.; Barzotto, I.L.M.; Vieira, L.; Sene, A.; Radi, P.A.; Fraga, S.; Bessa, M.J.; Teixeira, J.P.; Carvalho, I.C.S.; da Silva, N.S. Tribocorrosion studies on diamond-like carbon film deposited by PECVD on 304 stainless steel in simulated body fluid. *Biomed. Phys. Eng. Express* **2019**, *5*, 045012. [[CrossRef](#)]
42. Gracia-Escosa, E.; Garcia, I.; Sanchez-Lopez, J.; Abad, M.; Mariscal, A.; Arenas, M.; de Damborenea, J.; Conde, A. Tribocorrosion behavior of TiB_xC_y/a-C nanocomposite coating in strong oxidant disinfectant solutions. *Surf. Coat. Technol.* **2015**, *263*, 78–85. [[CrossRef](#)]
43. Wu, J.; Wu, G.; Kou, X.; Lu, Z.; Zhang, G.; Wu, Z. Probing Tribological Behaviors of Cr-DLC in Corrosion Solution by Tailoring Sliding Interface. *Tribol. Lett.* **2020**, *68*, 95. [[CrossRef](#)]
44. Shen, Y.; Luo, J.; Liao, B.; Chen, L.; Zhang, X.; Zhao, Y.; Pang, P.; Zeng, X. Enhanced Anti-Tribocorrosion Performance of Ti-DLC Coatings Deposited by Filtered Cathodic Vacuum Arc with the Optimization of Bias Voltage. *Coatings* **2022**, *12*, 697. [[CrossRef](#)]
45. Sun, J.; Tang, Y.; Xu, X.; Li, Z.; Su, F. Synthesis of Nitrogen-Doped Diamond-Like Carbon Films Produced by Plasma-Enhanced Chemical Vapor Deposition and their Tribocorrosion Behavior in Hanks' Solution. *J. Mater. Eng. Perform.* **2022**, *31*, 8334–8345. [[CrossRef](#)]
46. Cui, M.; Pu, J.; Liang, J.; Wang, L.; Zhang, G.; Xue, Q. Corrosion and tribocorrosion performance of multilayer diamond-like carbon film in NaCl solution. *RSC Adv.* **2015**, *5*, 104829–104840. [[CrossRef](#)]
47. Pu, J.; Wang, J.; He, D.; Wan, S. Corrosion and tribocorrosion behaviour of super-thick diamond-like carbon films deposited on stainless steel in NaCl solution. *Surf. Interface Anal.* **2016**, *48*, 360–367. [[CrossRef](#)]
48. Wang, Q.; Zhou, F.; Wang, C.; Yuen, M.-F.; Wang, M.; Qian, T.; Matsumoto, M.; Yan, J. Comparison of tribological and electrochemical properties of TiN, CrN, TiAlN and a-C:H coatings in simulated body fluid. *Mater. Chem. Phys.* **2015**, *158*, 74–81. [[CrossRef](#)]
49. Lou, B.-S.; Rahmadtulloh, I.; Wang, C.-J.; Wang, W.-H.; Lee, J.-W. Tribocorrosion behaviors of VNbMoTaWCr high entropy alloy coatings. *Surf. Coat. Technol.* **2023**, *476*, 130250. [[CrossRef](#)]
50. Tasdemir, M.; Senaslan, F.; Celik, A. Wear, Corrosion and Tribocorrosion Behavior of Polyurethane and Polyvinylpyrrolidone Blends as Coating for Corrosion Protection of AISI 316L Stainless Steel. *Int. J. Electrochem. Sci.* **2021**, *16*, 210510. [[CrossRef](#)]
51. Lin, Q.; Wang, X.; Cai, M.; Yan, H.; Zhao, Z.; Fan, X.; Zhu, M. Enhancement of Si₃N₄@MoS₂ core-shell structure on wear/corrosion resistance of epoxy resin/polyacrylate IPN composite coating. *Appl. Surf. Sci.* **2021**, *568*, 150938. [[CrossRef](#)]
52. Lajevardi, S.A.; Shahrabi, T.; Szpunar, J.A. Tribological Properties of Functionally Graded Ni-Al₂O₃ Nanocomposite Coating. *J. Electrochem. Soc.* **2017**, *164*, D275–D281. [[CrossRef](#)]
53. Offoiach, R.; Lekka, M.; Lanzutti, A.; Martínez-Nogués, V.; Vega, J.M.; García-Lecina, E.; Fedrizzi, L. Tribocorrosion study of Ni/B electrodeposits with low B content. *Surf. Coat. Technol.* **2019**, *369*, 1–15. [[CrossRef](#)]
54. Lee, H.B. Synergy Between Corrosion and Wear of Electrodeposited Ni–W Coating. *Tribol. Lett.* **2013**, *50*, 407–419. [[CrossRef](#)]
55. Hassani, S.; Raeissi, K.; Azzi, M.; Li, D.; Golozar, M.; Szpunar, J. Improving the corrosion and tribocorrosion resistance of Ni-Co nanocrystalline coatings in NaOH solution. *Corros. Sci.* **2009**, *51*, 2371–2379. [[CrossRef](#)]
56. Malfatti, C.; Veit, H.; Santos, C.; Metzner, M.; Hololeczek, H.; Bonino, J. Heat Treated NiP-SiC Composite Coatings: Elaboration and Tribocorrosion Behaviour in NaCl Solution. *Tribol. Lett.* **2009**, *36*, 165–173. [[CrossRef](#)]
57. Benea, L. Electrodeposition and tribocorrosion behaviour of ZrO₂-Ni composite coatings. *J. Appl. Electrochem.* **2009**, *39*, 1671–1681. [[CrossRef](#)]

58. Chun-Ying, L.; Wei-Ti, M.; Ming-Der, G.; Hung-Bin, L. A study on the corrosion and wear behavior of nanocrystalline Ni-Mo electrodeposited coatings. *Surf. Coat. Technol.* **2019**, *366*, 286–295. [[CrossRef](#)]
59. Benea, L.; Basa, S.; Danaila, E.; Caron, N.; Raquet, O.; Ponthiaux, P.; Celis, J. Fretting and wear behaviors of Ni/nano-WC composite coatings in dry and wet conditions. *Mater. Des.* **2015**, *65*, 550–558. [[CrossRef](#)]
60. Fathollahzade, N.; Raeissi, K. A tribocorrosion study of cobalt–tungsten electrodeposited coating with a mixed amorphous/nanocrystalline structure. *Int. J. Surf. Eng. Coat.* **2016**, *94*, 328–335. [[CrossRef](#)]
61. Rajabi, M.; Tahmasebi, K.; Ehteshamzadeh, M.; Soroushian, S. Tribological and magnetic behaviour of Ni-P coating modified with NiO nanoparticles. *Tribol. Mater. Surf. Interfaces* **2021**, *15*, 243–251. [[CrossRef](#)]
62. Salicio-Paz, A.; Dalmau, A.; Grande, H.; Iriarte, A.; Sort, J.; Pellicer, E.; Fornell, J.; García-Lecina, E. Impact of the multilayer approach on the tribocorrosion behaviour of nanocrystalline electroless nickel coatings obtained by different plating modes. *Wear* **2020**, *456–457*, 203384. [[CrossRef](#)]
63. Vitry, V.; Bonin, L. Effect of temperature on ultrasound-assisted electroless nickel-boron plating. *Ultrason. Sonochem.* **2019**, *56*, 327–336. [[CrossRef](#)]
64. Tabatabaei, F.; Raeissi, K.; Saatchi, A.; Kazmanlı, K.; Ürgen, M. Effect of heat treatment on tribocorrosion of nanostructure Ni-P coatings. *Surf. Eng.* **2013**, *29*, 671–676. [[CrossRef](#)]
65. Wang, J.; Bian, D.; Liu, Y.; Zhao, Y.; Tang, H. Influence of aluminum phosphate on the tribocorrosion performance of chemically bonded phosphate ceramic coatings. *Mater. Corros. Werkst. Korros.* **2021**, *72*, 1677–1686. [[CrossRef](#)]
66. Li, T.; Li, L.; Qi, J.; Chen, F. Corrosion protection of Ti6Al4V by a composite coating with a plasma electrolytic oxidation layer and sol-gel layer filled with graphene oxide. *Prog. Org. Coat.* **2020**, *144*, 105632. [[CrossRef](#)]
67. Da, B.; Yaxuan, L.; Vasu, A.T.; Yongxin, G.; Hao, T.; Yongwu, Z.; Yongguang, W. Improving tribocorrosion performance of chemically bonded ceramic phosphate coating reinforced by GO-ZnO. *Ceram. Int.* **2021**, *47*, 15722–15731. [[CrossRef](#)]
68. Ripoll, M.R.; Torres, H. Chapter 6–Tribocorrosion of hard coatings and thin films. In *Tribocorrosion*; Siddaiah, A., Ramachandran, R., Menezes, P.L., Eds.; Academic Press: Cambridge, MA, USA, 2021; pp. 127–171, ISBN 978-0-12-818916-0.
69. Łapaj, Ł.; Wendland, J.; Markuszewski, J.; Mróz, A.; Wiśniewski, T. Retrieval analysis of titanium nitride (TiN) coated prosthetic femoral heads articulating with polyethylene. *J. Mech. Behav. Biomed. Mater.* **2016**, *55*, 127–139. [[CrossRef](#)]
70. Pougoum, F.; Qian, J.; Martinu, L.; Klemberg-Sapieha, J.; Zhou, Z.; Li, K.Y.; Savoie, S.; Lacasse, R.; Potvin, E.; Schulz, R. Study of corrosion and tribocorrosion of Fe₃Al-based duplex PVD/HVOF coatings against alumina in NaCl solution. *Surf. Coat. Technol.* **2019**, *357*, 774–783. [[CrossRef](#)]
71. Kovacı, H.; Bozkurt, Y.B.; Yetim, A.F.; Baran, Ö.; Çelik, A. Corrosion and tribocorrosion properties of duplex surface treatments consisting of plasma nitriding and DLC coating. *Tribol. Int.* **2021**, *156*, 106823. [[CrossRef](#)]
72. Bayon, R.; Nevshupa, R.; Zubizarreta, C.; de Gopegui, U.; Barriga, J.; Igartua, A. Characterisation of tribocorrosion behaviour of multilayer PVD coatings. *Anal. Bioanal. Chem.* **2010**, *396*, 2855–2862. [[CrossRef](#)]
73. Bai, W.Q.; Li, L.L.; Xie, Y.J.; Liu, D.G.; Wang, X.L.; Jin, G.; Tu, J.P. Corrosion and tribocorrosion performance of M (M Ta, Ti) doped amorphous carbon multilayers in Hank’s solution. *Surf. Coat. Technol.* **2016**, *305*, 11–22. [[CrossRef](#)]
74. Çomaklı, O. Improved structural, mechanical, corrosion and tribocorrosion properties of Ti45Nb alloys by TiN, TiAlN monolayers, and TiAlN/TiN multilayer ceramic films. *Ceram. Int.* **2021**, *47*, 4149–4156. [[CrossRef](#)]
75. Çaha, I.; Alves, A.C.; Affonso, L.J.; da Silva, J.H.D.; Rodrigues, I.R.; Grandini, C.R.; Rocha, L.A.; Pinto, A.M.P.; Lisboa-Filho, P.N.; Toptan, F. Degradation behaviour of Ti-12Nb alloy coated with ZnO/TiN double layer. *Surf. Coat. Technol.* **2021**, *413*, 127104. [[CrossRef](#)]
76. Sun, Y.; Dearnley, P.A.; Mallia, B. Response of duplex Cr(N)/S and Cr(C)/S coatings on 316L stainless steel to tribocorrosion in 0.89% NaCl solution under plastic contact conditions: Response of Duplex Cr(N)/S and Cr(C)/S Coatings. *J. Biomed. Mater. Res. B Appl. Biomater.* **2017**, *105*, 1503–1513. [[CrossRef](#)]
77. Mazzonello, A.; Buhagiar, J.; Chetcuti, R.; Dearnley, P.; Valsesia, A.; Colpo, P.; Mallia, B. A tribocorrosion appraisal of a dual layer PVD coated CoCrMo alloy tribopair. *Surf. Coat. Technol.* **2022**, *442*, 128341. [[CrossRef](#)]
78. Chetcuti, R.; Dearnley, P.; Mazzonello, A.; Buhagiar, J.; Mallia, B. Tribocorrosion response of duplex layered CoCrMoC/CrN and CrN/CoCrMoC coatings on implant grade 316LVM stainless steel. *Surf. Coat. Technol.* **2020**, *384*, 125313. [[CrossRef](#)]
79. Naghibi, S.; Raeissi, K.; Fathi, M. Corrosion and tribocorrosion behavior of Ti/TiN PVD coating on 316L stainless steel substrate in Ringer’s solution. *Mater. Chem. Phys.* **2014**, *148*, 614–623. [[CrossRef](#)]
80. Zhao, C.; Zhu, Y.; Yuan, Z.; Li, J. Structure and tribocorrosion behavior of Ti/TiN multilayer coatings in simulated body fluid by arc ion plating. *Surf. Coat. Technol.* **2020**, *403*, 126399. [[CrossRef](#)]
81. Beliardouh, N.; Ramoul, C.; Nouveau, C.; Kaleli, E.; Montagne, A. Synthesis and tribocorrosion performances of multilayer (Ta/ZrN)_n coatings. *Thin Solid Film.* **2022**, *749*, 139184. [[CrossRef](#)]
82. de Frutos, A.; Arenas, M.; Fuentes, G.; Rodriguez, R.; Martinez, R.; Avelar-Batista, J.; de Damborenea, J. Tribocorrosion behaviour of duplex surface treated AISI 304 stainless steel. *Surf. Coat. Technol.* **2010**, *204*, 1623–1630. [[CrossRef](#)]
83. Zhao, G.-H.; Aune, R.E.; Espallargas, N. Tribocorrosion studies of metallic biomaterials: The effect of plasma nitriding and DLC surface modifications. *J. Mech. Behav. Biomed. Mater.* **2016**, *63*, 100–114. [[CrossRef](#)]
84. Uzun, Y. Tribocorrosion properties of plasma nitrided, Ti-DLC coated and duplex surface treated AISI 316L stainless steel. *Surf. Coat. Technol.* **2022**, *441*, 128587. [[CrossRef](#)]

85. Grabarczyk, J.; Gaj, J.; Pazik, B.; Kaczorowski, W.; Januszewicz, B. Tribocorrosion behavior of Ti₆Al₄V alloy after thermo-chemical treatment and DLC deposition for biomedical applications. *Tribol. Int.* **2021**, *153*, 106560. [[CrossRef](#)]
86. Lopez-Ortega, A.; de Viteri, V.; Alves, S.; Mendoza, G.; Fuentes, E.; Mitran, V.; Cimpean, A.; Dan, I.; Vela, A.; Bayon, R. Multifunctional TiO₂ coatings developed by plasma electrolytic oxidation technique on a Ti₂₀Nb₂₀Zr₄Ta alloy for dental applications. *Biomater. Adv.* **2022**, *138*, 212875. [[CrossRef](#)]
87. Rahmatian, B.; Ghasemi, H.M.; Sohi, M.H.; De Baets, P. Insight into tribocorrosion resistance and tribofilm formation on titanium boride coatings in a phosphate buffer saline solution. *J. Mater. Res. Technol.* **2023**, *27*, 6847–6862. [[CrossRef](#)]
88. Zhai, H.; Cui, S.; Li, S.; He, D.; Cheng, B.; Zhang, X.; Li, W.; Viktor, Z.; Seniuts, U. Tribocorrosion behaviors of Ti-based bulk metallic glass via laser shock peening in 3.5 wt % NaCl solutions. *Intermetallics* **2024**, *164*, 108127. [[CrossRef](#)]
89. Xu, L.; Zhang, D.; Su, H.; Yu, P.; Wan, Y.; Sun, H. Improving the tribocorrosion performance of plasma electrolytic oxidized coatings on AZ31B magnesium alloy using pullulan as an electrolyte additive. *Surf. Coat. Technol.* **2022**, *446*, 128754. [[CrossRef](#)]
90. Xu, L.; Fu, X.; Su, H.; Sun, H.; Li, R.; Wan, Y. Corrosion and tribocorrosion protection of AZ31B Mg alloy by a hydrothermally treated PEO/chitosan composite coating. *Prog. Org. Coat.* **2022**, *170*, 107002. [[CrossRef](#)]
91. Sourani, F.; Raeissi, K.; Enayati, M.; Kharaziha, M.; Hakimizad, A.; Blugan, G.; Salimijazi, H. Corrosion and tribocorrosion behavior of ZrO₂-Al₂O₃ composite coatings developed by plasma electrolytic oxidation for load-bearing implants. *J. Alloys Compd.* **2022**, *920*, 165856. [[CrossRef](#)]
92. Daavari, M.; Atapour, M.; Mohedano, M.; Arrabal, R.; Matykina, E.; Taherizadeh, A. Biotribology and biocorrosion of MWCNTs-reinforced PEO coating on AZ31B Mg alloy. *Surf. Interfaces* **2021**, *22*, 100850. [[CrossRef](#)]
93. Yang, J.; Gu, Y.; Zhou, X.; Zhang, Y. Tribocorrosion behavior and mechanism of micro-arc oxidation Ca/P coating on nanocrystallized magnesium alloys. *Mater. Corros. Werkst. Korros.* **2018**, *69*, 749–759. [[CrossRef](#)]
94. Xu, L.; Liu, N.; Cao, L.; Wan, Y. Influences of electrolytes on tribocorrosion performance of MAO coating on AZ31B magnesium alloy in simulated body fluid. *Int. J. Appl. Ceram. Technol.* **2021**, *18*, 1657–1669. [[CrossRef](#)]
95. Dalmau, A.; Buch, A.R.; Rovira, A.; Navarro-Laboulais, J.; Muñoz, A.I. Wear model for describing the time dependence of the material degradation mechanisms of the AISI 316L in a NaCl solution. *Wear* **2018**, *394–395*, 166–175. [[CrossRef](#)]
96. Papageorgiou, N.; von Bonin, A.; Espallargas, N. Tribocorrosion mechanisms of NiCrMo-625 alloy: An electrochemical modeling approach. *Tribol. Int.* **2014**, *73*, 177–186. [[CrossRef](#)]
97. Wang, K.; Wang, Y.; Yue, X.; Cai, W. Multiphysics modeling and uncertainty quantification of tribocorrosion in aluminum alloys. *Corros. Sci.* **2021**, *178*, 109095. [[CrossRef](#)]
98. Fallahnezhad, K.; Feyzi, M.; Ghadirinejad, K.; Hashemi, R.; Taylor, M. Finite element based simulation of tribocorrosion at the head-neck junction of hip implants. *Tribol. Int.* **2022**, *165*, 107284. [[CrossRef](#)]
99. Papageorgiou, N.; Mischler, S. Electrochemical Simulation of the Current and Potential Response in Sliding Tribocorrosion. *Tribol. Lett.* **2012**, *48*, 271–283. [[CrossRef](#)]
100. Guadalupe, S.; Cao, S.; Cantoni, M.; Chitty, W.-J.; Falcand, C.; Mischler, S. Applicability of a recently proposed tribocorrosion model to CoCr alloys with different carbides content. *Wear* **2017**, *376–377*, 203–211. [[CrossRef](#)]
101. Gilbert, J.L.; Mali, S.A.; Liu, Y. Area-dependent impedance-based voltage shifts during tribocorrosion of Ti-6Al-4V biomaterials: Theory and experiment. *Surf. Topogr. Metrol. Prop.* **2016**, *4*, 034002. [[CrossRef](#)]
102. Gilbert, J.L.; Zhu, D. A metallic biomaterial tribocorrosion model linking fretting mechanics, currents, and potentials: Model development and experimental comparison. *J. Biomed. Mater. Res. B Appl. Biomater.* **2020**, *108*, 3174–3189. [[CrossRef](#)]
103. Dalbert, V.; Mary, N.; Normand, B.; Verdu, C.; Saedlou, S. In situ determinations of the wear surfaces, volumes and kinetics of repassivation: Contribution in the understanding of the tribocorrosion behaviour of a ferritic stainless steel in various pH. *Tribol. Int.* **2020**, *150*, 106374. [[CrossRef](#)]
104. Fallahnezhad, K.; Feyzi, M.; Hashemi, R.; Taylor, M. The Role of the Assembly Force in the Tribocorrosion Behaviour of Hip Implant Head-Neck Junctions: An Adaptive Finite Element Approach. *Bioengineering* **2022**, *9*, 629. [[CrossRef](#)]
105. Cao, S.; Maldonado, S.; Mischler, S. Tribocorrosion of passive metals in the mixed lubrication regime: Theoretical model and application to metal-on-metal artificial hip joints. *Wear* **2015**, *324*, 55–63. [[CrossRef](#)]
106. Miyabe, S.; Fujii, N.; Fujimoto, S. Numerical Simulation of Tribocorrosion of CoCr Alloy and Ti with Galvanic Coupling in Simulated Body Fluid. *Mater. Trans.* **2021**, *62*, 1489–1494. [[CrossRef](#)]
107. von der Ohe, C.B.; Johnsen, R.; Espallargas, N. Modeling the multi-degradation mechanisms of combined tribocorrosion interacting with static and cyclic loaded surfaces of passive metals exposed to seawater. *Wear* **2010**, *269*, 607–616. [[CrossRef](#)]
108. Wang, H.; Liu, T.; Zhang, Y.; Zhu, Y.; Liu, F.; Wang, T. A Fully Coupled Tribocorrosion Simulation Method for Anchor Chain Considering Mechano-Electrochemical Interaction. *Lubricants* **2022**, *10*, 330. [[CrossRef](#)]
109. Wang, W.; Wang, K.; Zhang, Z.; Chen, J.; Mou, T.; Michel, F.; Xin, H.; Cai, W. Ultrahigh tribocorrosion resistance of metals enabled by nano-layering. *ACTA Mater.* **2021**, *206*, 116609. [[CrossRef](#)]
110. Olsson, C.-O.A.; Munoz, A.N.I.; Cao, S.; Mischler, S. Modeling Current Transients in a Reciprocal Motion Tribocorrosion Experiment. *J. Electrochem. Soc.* **2021**, *168*, 031503. [[CrossRef](#)]
111. Mary, N.; Ter-Ovanesian, B.; Normand, B. Growth mechanism and repassivation kinetic determinations on stainless steel under sliding: Role of the solution pH and dissolved oxygen concentration. *Wear* **2020**, *460–461*, 203478. [[CrossRef](#)]
112. Ghanbarzadeh, A.; Salehi, F.M.; Bryant, M.; Neville, A. A New Asperity-Scale Mechanistic Model of Tribocorrosive Wear: Synergistic Effects of Mechanical Wear and Corrosion. *J. Tribol.* **2019**, *141*, 021601. [[CrossRef](#)]

113. Stachowiak, A.; Zwierzycki, W. Analysis of the tribocorrosion mechanisms in a pin-on-plate combination on the example of AISI304 steel. *Wear* **2012**, *294*, 277–285. [[CrossRef](#)]
114. Stachowiak, A.; Tyczewski, P.; Zwierzycki, W. The application of wear maps for analyzing the results of research into tribocorrosion. *Wear* **2016**, *352–353*, 146–154. [[CrossRef](#)]
115. Ramachandran, R. Machine learning model to cluster and map tribocorrosion regimes in feature space. *arXiv* **2020**, arXiv:2006.06252. [[CrossRef](#)]
116. Ramachandran, R. Machine Learning Model to Map Tribocorrosion Regimes in Feature Space. *Coatings* **2021**, *11*, 450. [[CrossRef](#)]
117. Jiang, J.; Stack, M.M.; Neville, A. Modelling the tribo-corrosion interaction in aqueous sliding conditions. *Tribol. Int.* **2002**, *35*, 669–679. [[CrossRef](#)]
118. Maldonado, S.G.; Mischler, S.; Cantoni, M.; Chitty, W.J.; Falcand, C.; Hertz, D. Mechanical and chemical mechanisms in the tribocorrosion of a Stellite type alloy. *Wear* **2013**, *308*, 213–221. [[CrossRef](#)]
119. Dowson, D. Tribological principles in metal-on-metal hip joint design. *Proc. Inst. Mech.Eng. Part H J. Eng. Med.* **2006**, *220*, 161–171. [[CrossRef](#)] [[PubMed](#)]
120. Soltanahmadi, S.; Morina, A.; van Eijk, M.C.; Nedelcu, I.; Neville, A. Tribochemical study of micropitting in tribocorrosive lubricated contacts: The influence of water and relative humidity. *Tribol. Int.* **2017**, *107*, 184–198. [[CrossRef](#)]
121. Wang, W.; Mraied, H.; Diyatmika, W.; Chu, J.; Li, L.; Cai, W. Effects of nanoscale chemical heterogeneity on the wear, corrosion, and tribocorrosion resistance of Zr-based thin film metallic glasses. *Surf. Coat. Technol.* **2020**, *402*, 126324. [[CrossRef](#)]
122. Zou, J.; Wang, Z.; Ma, Y.; Yan, Y.; Qiao, L. Role of gradient nano-structured surface in collapsed pitting corrosion on AISI 316L stainless steel during tribocorrosion. *Corros. Sci.* **2022**, *197*, 110043. [[CrossRef](#)]
123. Liu, Z.; Liu, E.; Du, S.; Zhang, J.; Wang, L.; Du, H.; Cai, H. Tribocorrosion Behavior of Typical Austenitic, Martensitic, and Ferritic Stainless Steels in 3.5% NaCl Solution. *J. Mater. Eng. Perform.* **2021**, *30*, 6284–6296. [[CrossRef](#)]
124. Tan, L.; Wang, Z.; Ma, Y. Tribocorrosion Behavior and Degradation Mechanism of 316L Stainless Steel in Typical Corrosive Media. *Acta Metall. Sin. Engl. Lett.* **2021**, *34*, 813–824. [[CrossRef](#)]
125. Sousa, J.M.; Alves, A.C.; Toptan, F.; Ariza, E.; Guedes, A. Corrosion and Tribocorrosion Behavior of Ti-B4C Composites Joined with TiCuNi Brazing Alloy. *J. Mater. Eng. Perform.* **2019**, *28*, 4972–4982. [[CrossRef](#)]
126. Mraied, H.; Cai, W. The effects of Mn concentration on the tribocorrosion resistance of Al–Mn alloys. *Wear* **2017**, *380–381*, 191–202. [[CrossRef](#)]
127. Obadele, B.A.; Andrews, A.; Shongwe, M.B.; Olubambi, P.A. Tribocorrosion behaviours of AISI 310 and AISI 316 austenitic stainless steels in 3.5% NaCl solution. *Mater. Chem. Phys.* **2016**, *171*, 239–246. [[CrossRef](#)]
128. Sun, Y.; Rana, V. Tribocorrosion behaviour of AISI 304 stainless steel in 0.5M NaCl solution. *Mater. Chem. Phys.* **2011**, *129*, 138–147. [[CrossRef](#)]
129. Kossman, S.; Coelho, L.B.; Mejias, A.; Montagne, A.; Van Gorp, A.; Coorevits, T.; Touzin, M.; Poorteman, M.; Olivier, M.-G.; Iost, A.; et al. Impact of industrially applied surface finishing processes on tribocorrosion performance of 316L stainless steel. *Wear* **2020**, *456–457*, 203341. [[CrossRef](#)]
130. Zhang, Y.; Yin, X.; Yan, Y.; Wang, J.; Yan, F. Tribocorrosion behaviors of 304SS: Effect of solution pH. *RSC Adv.* **2015**, *5*, 17676–17682. [[CrossRef](#)]
131. Zou, J.; Wang, Z.; Ma, Y.; Tan, L. Tribocorrosion Behavior and Degradation Mechanism of 316L Stainless Steel in Alkaline Solution: Effect of Tribo-Film. *ACTA Metall. Sin. Engl. Lett.* **2022**, *35*, 1365–1375. [[CrossRef](#)]
132. Xin, L.; Jiang, L. Effects of Normal Force on the Tribocorrosion Behavior of a Nickel-Based Superalloy in Alkaline Solution: An Electrochemical Study. *Materials* **2020**, *13*, 3959. [[CrossRef](#)]
133. Du, J.; Cao, S.; Igual Munoz, A.; Mischler, S. Tribological and tribocorrosion behavior of nickel sliding against oxide ceramics. *Wear* **2019**, *426–427*, 1496–1506. [[CrossRef](#)]
134. Espallargas, N.; Mischler, S. Tribocorrosion behaviour of overlay welded Ni-Cr 625 alloy in sulphuric and nitric acids: Electrochemical and chemical effects. *Tribol. Int.* **2010**, *43*, 1209–1217. [[CrossRef](#)]
135. Balla, V.K.; Das, M. Advances in Wear and Tribocorrosion Testing of Artificial Implants and Materials: A Review. *Trends Biomater. Artif. Organs* **2017**, *31*, 150.
136. Zheng, Y.; Bashandeh, K.; Shakil, A.; Jha, S.; Polycarpou, A.A. Review of dental tribology: Current status and challenges. *Tribol. Int.* **2022**, *166*, 107354. [[CrossRef](#)]
137. Zindani, D.; Kumar, K.; Paulo Davim, J. Metallic biomaterials—A review. In *Mechanical Behaviour of Biomaterials*; Elsevier: Amsterdam, The Netherlands, 2019; pp. 83–99, ISBN 978-0-08-102174-3.
138. Siddaiah, A. Understanding the Tribocorrosion Behavior of Engineered Surfaces. Ph.D. Thesis, University of Nevada, Reno, NV, USA, 2020; 163p.
139. Ferreira, D.; Almeida, S.; Soares, R.; Juliani, L.; Bracarense, A.; Lins, V.; Junqueira, R. Synergism between mechanical wear and corrosion on tribocorrosion of a titanium alloy in a Ringer solution. *J. Mater. Res. Technol.* **2019**, *8*, 1593–1600. [[CrossRef](#)]
140. Shahmohammadi, M.; Sun, Y.; Yuan, J.C.-C.; Mathew, M.T.; Sukotjo, C.; Takoudis, C.G. In vitro corrosion behavior of coated Ti₆Al₄V with TiO₂, ZrO₂, and TiO₂/ZrO₂ mixed nanofilms using atomic layer deposition for dental implants. *Surf. Coat. Technol.* **2022**, *444*, 128686. [[CrossRef](#)]

141. Alves, S.A.; Patel, S.B.; Sukotjo, C.; Mathew, M.T.; Filho, P.N.; Celis, J.-P.; Rocha, L.A.; Shokuhfar, T. Synthesis of calcium-phosphorous doped TiO₂ nanotubes by anodization and reverse polarization: A promising strategy for an efficient biofunctional implant surface. *Appl. Surf. Sci.* **2017**, *399*, 682–701. [[CrossRef](#)]
142. Tobin, E.J. Recent coating developments for combination devices in orthopedic and dental applications: A literature review. *Adv. Drug Deliv. Rev.* **2017**, *112*, 88–100. [[CrossRef](#)]
143. Ribeiro, A.R.; Gemini-Piperni, S.; Travassos, R.; Lemgruber, L.; Silva, R.C.; Rossi, A.L.; Farina, M.; Anselme, K.; Shokuhfar, T.; Shahbazian-Yassar, R.; et al. Trojan-Like Internalization of Anatase Titanium Dioxide Nanoparticles by Human Osteoblast Cells. *Sci. Rep.* **2016**, *6*, 23615. [[CrossRef](#)]
144. Yang, R.; Hao, Y.; Li, S. Development and application of low-modulus biomedical titanium alloy Ti2448. *Biomed. Eng. Trends* **2011**, *10*, 225–247.
145. Mastnak, T.; Maver, U.; Finšgar, M. Addressing the Needs of the Rapidly Aging Society through the Development of Multifunctional Bioactive Coatings for Orthopedic Applications. *Int. J. Mol. Sci.* **2022**, *23*, 2786. [[CrossRef](#)]
146. Brooks, E.K.; Brooks, R.P.; Ehrensberger, M.T. Effects of simulated inflammation on the corrosion of 316L stainless steel. *Mater. Sci. Eng. C* **2017**, *71*, 200–205. [[CrossRef](#)]
147. Rafiq, N.M.; Wang, W.; Liew, S.L.; Chua, C.S.; Wang, S. A review on multifunctional bioceramic coatings in hip implants for osteointegration enhancement. *Appl. Surf. Sci. Adv.* **2023**, *13*, 100353. [[CrossRef](#)]
148. Manam, N.S.; Harun, W.S.W.; Shri, D.N.A.; Ghani, S.A.C.; Kurniawan, T.; Ismail, M.H.; Ibrahim, M.H.I. Study of corrosion in biocompatible metals for implants: A review. *J. Alloys Compd.* **2017**, *701*, 698–715. [[CrossRef](#)]
149. Nicholson, J.W. Titanium Alloys for Dental Implants: A Review. *Prosthesis* **2020**, *2*, 11. [[CrossRef](#)]
150. Li, J.; He, X.; Zhang, G.; Hang, R.; Huang, X.; Tang, B.; Zhang, X. Electrochemical corrosion, wear and cell behavior of ZrO₂/TiO₂ alloyed layer on Ti-6Al-4V. *Bioelectrochemistry* **2018**, *121*, 105–114. [[CrossRef](#)] [[PubMed](#)]
151. Alhamad, M.; Barão, V.A.R.; Sukotjo, C.; Cooper, L.F.; Mathew, M.T. Ti-Ions and/or Particles in Saliva Potentially Aggravate Dental Implant Corrosion. *Materials* **2021**, *14*, 5733. [[CrossRef](#)] [[PubMed](#)]
152. Chellappa, M.; Vijayalakshmi, U. Improved corrosion resistant and mechanical behavior of distinct composite coatings (silica/titania/zirconia) on Ti-6Al-4V deposited by EPD. *J. Asian Ceram. Soc.* **2017**, *5*, 326–333. [[CrossRef](#)]
153. Romanos, G.; Fischer, G.; Delgado-Ruiz, R. Titanium Wear of Dental Implants from Placement, under Loading and Maintenance Protocols. *Int. J. Mol. Sci.* **2021**, *22*, 1067. [[CrossRef](#)]
154. Elias, C.N.; Fernandes, D.J.; Resende, C.R.S.; Roestel, J. Mechanical properties, surface morphology and stability of a modified commercially pure high strength titanium alloy for dental implants. *Dent. Mater.* **2015**, *31*, e1–e13. [[CrossRef](#)]
155. Ji, X.; Luo, C.; Jin, J.; Zhang, Y.; Sun, Y.; Fu, L. Tribocorrosion performance of 316L stainless steel enhanced by laser clad 2-layer coating using Fe-based amorphous powder. *J. Mater. Res. Technol.* **2022**, *17*, 612–621. [[CrossRef](#)]
156. Ji, X.; Luo, C.; Sun, Y.; Zhao, J. Corrosive wear of multi-layer Fe-based coatings laser clad from amorphous powders. *Wear* **2019**, *438–439*, 203113. [[CrossRef](#)]
157. Luo, C.; Ji, X.; Ji, C.; Zhang, Y.; Wang, H. Tribocorrosion of Fe-Based Amorphous Coating in Simulated Body Fluids. *Lubricants* **2018**, *6*, 37. [[CrossRef](#)]
158. Kirmanidou, Y.; Sidira, M.; Drosou, M.-E.; Bennani, V.; Bakopoulou, A.; Tsouknidas, A.; Michailidis, N.; Michalakis, K. New Ti-Alloys and Surface Modifications to Improve the Mechanical Properties and the Biological Response to Orthopedic and Dental Implants: A Review. *BioMed Res. Int.* **2016**, *2016*, 2908570. [[CrossRef](#)]
159. Costa, R.C.; Abdo, V.L.; Mendes, P.H.C.; Mota-Veloso, I.; Bertolini, M.; Mathew, M.T.; Barão, V.A.R.; Souza, J.G.S. Microbial Corrosion in Titanium-Based Dental Implants: How Tiny Bacteria Can Create a Big Problem? *J. Bio-Tribo-Corros.* **2021**, *7*, 136. [[CrossRef](#)]
160. Shemtov-Yona, K.; Rittel, D. On the mechanical integrity of retrieved dental implants. *J. Mech. Behav. Biomed. Mater.* **2015**, *49*, 290–299. [[CrossRef](#)]
161. Dong, H.; Liu, H.; Zhou, N.; Li, Q.; Yang, G.; Chen, L.; Mou, Y. Surface Modified Techniques and Emerging Functional Coating of Dental Implants. *Coatings* **2020**, *10*, 1012. [[CrossRef](#)]
162. Richard, C.; Kowandy, C.; Landoulsi, J.; Geetha, M.; Ramasawmy, H. Corrosion and wear behavior of thermally sprayed nano ceramic coatings on commercially pure Titanium and Ti-13Nb-13Zr substrates. *Int. J. Refract. Met. Hard Mater.* **2010**, *28*, 115–123. [[CrossRef](#)]
163. Visentin, F.; Galenda, A.; Fabrizio, M.; Battiston, S.; Brianese, N.; Gerbasi, R.; Zin, V.; El Habra, N. Assessment of synergistic effects of LP-MOCVD TiO₂ and Ti surface finish for dental implant purposes. *Appl. Surf. Sci.* **2019**, *490*, 568–579. [[CrossRef](#)]
164. Mezger, P.R.; Creugers, N.H.J. Titanium nitride coatings in clinical dentistry. *J. Dent.* **1992**, *20*, 342–344. [[CrossRef](#)]
165. Alves, S.; Bayon, R.; Igartua, A.; de Viteri, V.; Rocha, L. Tribocorrosion behaviour of anodic titanium oxide films produced by plasma electrolytic oxidation for dental implants. *Lubr. Sci.* **2014**, *26*, 500–513. [[CrossRef](#)]
166. Alves, A.C.; Oliveira, F.; Wenger, F.; Ponthiaux, P.; Celis, J.-P.; Rocha, L.A. Tribocorrosion behaviour of anodic treated titanium surfaces intended for dental implants. *J. Phys. Appl. Phys.* **2013**, *46*, 404001. [[CrossRef](#)]
167. Toptan, F.; Alves, A.; Pinto, A.; Ponthiaux, P. Tribocorrosion behavior of bio-functionalized highly porous titanium. *J. Mech. Behav. Biomed. Mater.* **2017**, *69*, 144–152. [[CrossRef](#)] [[PubMed](#)]
168. Costa, A.I.; Viana, F.; Toptan, F. Preliminary tribocorrosion evaluation of bio-functionalized Ti doped with Ca-P-Sr. *Mater. Lett.* **2021**, *283*, 128775. [[CrossRef](#)]

169. Rodrigues, N.; Alves, A.; Toptan, F.; Rocha, L. Preliminary investigation on the tribocorrosion behaviour of nanotubular structured Ti6Al4V surfaces. *Mater. Lett.* **2018**, *213*, 214–217. [CrossRef]
170. Costa, A.I.; Sousa, L.; Alves, A.C.; Toptan, F. Tribocorrosion behaviour of bio-functionalized porous Ti surfaces obtained by two-step anodic treatment. *Corros. Sci.* **2020**, *166*, 108467. [CrossRef]
171. Sousa, L.; Mendes, A.; Pinto, A.; Toptan, F.; Alves, A. Influence of Calcium Acetate Concentration in Electrolyte on Tribocorrosion Behaviour of MAO Treated Titanium. *Metals* **2021**, *11*, 1985. [CrossRef]
172. Caha, I.; Alves, A.; Chirico, C.; Pinto, A.; Tsipas, S.; Gordo, E.; Toptan, F. A promising method to develop TiO₂-based nanotubular surfaces on Ti-40Nb alloy with enhanced adhesion and improved tribocorrosion resistance. *Appl. Surf. Sci.* **2021**, *542*, 148658. [CrossRef]
173. Caha, I.; Alves, A.; Chirico, C.; Pinto, A.; Tsipas, S.; Gordo, E.; Toptan, F. Tribocorrosion-Resistant Ti40Nb-TiN Composites Having TiO₂-Based Nanotubular Surfaces. *ACS Biomater. Sci. Eng.* **2022**, *8*, 1816–1828. [CrossRef] [PubMed]
174. Caha, I.; Alves, A.C.; Chirico, C.; Pinto, A.M.; Tsipas, S.; Gordo, E.; Toptan, F. Improved tribocorrosion behavior on bio-functionalized β -type titanium alloy by the pillar effect given by TiN reinforcements. *Surf. Coat. Technol.* **2021**, *415*, 127122. [CrossRef]
175. Garcia-Cabezón, C.; Rodríguez-Méndez, M.L.; Borrás, V.A.; Bayón, R.; Salvo-Comino, C.; Garcia-Hernandez, C.; Martin-Pedrosa, F. Improvements in tribological and anticorrosion performance of porous Ti-6Al-4V via PEO coating. *Friction* **2021**, *9*, 1303–1318. [CrossRef]
176. Zuo, Y.; Li, T.; Jiang, X.; Wu, M.; Zhang, Y.; Chen, F. Tribocorrosion behavior of Ca-P MAO coatings on Ti6Al4V alloy at various applied voltages. *J. Mater. Res.* **2020**, *35*, 444–453. [CrossRef]
177. Zuo, Y.; Li, T.; Yu, P.; Zhao, Z.; Chen, X.; Zhang, Y.; Chen, F. Effect of graphene oxide additive on tribocorrosion behavior of MAO coatings prepared on Ti₆Al₄V alloy. *Appl. Surf. Sci.* **2019**, *480*, 26–34. [CrossRef]
178. He, B.; Xin, C.; Chen, Y.; Xu, Y.; Zhao, Q.; Hou, Z.; Tang, Y.; Liu, H.; Su, X.; Zhao, Y. Biological performance and tribocorrosion behavior of in-situ synthesized CuxO/TiO₂ coatings. *Appl. Surf. Sci.* **2022**, *600*, 154096. [CrossRef]
179. Aliofkhaezrai, M.; Macdonald, D.D.; Matykina, E.; Parfenov, E.V.; Egorkin, V.S.; Curran, J.A.; Troughton, S.C.; Sinebryukhov, S.L.; Gnednikov, S.V.; Lampke, T.; et al. Review of plasma electrolytic oxidation of titanium substrates: Mechanism, properties, applications and limitations. *Appl. Surf. Sci. Adv.* **2021**, *5*, 100121. [CrossRef]
180. Revathi, A.; Borrás, A.D.; Muñoz, A.I.; Richard, C.; Manivasagam, G. Degradation mechanisms and future challenges of titanium and its alloys for dental implant applications in oral environment. *Mater. Sci. Eng. C* **2017**, *76*, 1354–1368. [CrossRef] [PubMed]
181. Hart, A.J.; Satchithananda, K.; Liddle, A.D.; Sabah, S.A.; McRobbie, D.; Henckel, J.; Cobb, J.P.; Skinner, J.A.; Mitchell, A.W. Pseudotumors in Association with Well-Functioning Metal-on-Metal Hip Prostheses: A Case-Control Study Using Three-Dimensional Computed Tomography and Magnetic Resonance Imaging. *J. Bone Jt. Surg. Am.* **2012**, *94*, 317–325. [CrossRef] [PubMed]
182. Urban, R.M.; Jacobs, J.J.; Tomlinson, M.J.; Gavrilovic, J.; Black, J.; Peoc'h, M. Dissemination of Wear Particles to the Liver, Spleen, and Abdominal Lymph Nodes of Patients with Hip or Knee Replacement*. *J. Bone Jt. Surg. Am.* **2000**, *82*, 457. [CrossRef] [PubMed]
183. Concerns about Metal-on-Metal Hip Implants. In US Food & Drug Administration. Available online: <https://www.fda.gov/medical-devices/metal-metal-hip-implants/concerns-about-metal-metal-hip-implants> (accessed on 12 November 2023).
184. Boulila, A.; Bouzid, L.; Ayadi, M. Chapter 6—Failure of total hip arthroplasty (THA): State of the art. In *Medical and Healthcare Robotics*; Boubaker, O., Ed.; Academic Press: Cambridge, MA, USA, 2023; pp. 157–181, ISBN 978-0-443-18460-4.
185. Cheng, K.-Y.; Bijukumar, D.; Runa, M.; McNallan, M.; Mathew, M. Chapter 5—Tribocorrosion aspects of implant coatings: Hip replacements. In *Tribocorrosion*; Siddaiah, A., Ramachandran, R., Menezes, P.L., Eds.; Academic Press: Cambridge, MA, USA, 2021; pp. 93–126, ISBN 978-0-12-818916-0.
186. Swaminathan, V.; Gilbert, J. Fretting corrosion of CoCrMo and Ti₆Al₄V interfaces. *Biomaterials* **2012**, *33*, 5487–5503. [CrossRef]
187. Norman, T.L.; Denen, J.E.; Land, A.J.; Kienitz, D.M.; Fehring, T.A. Taper-Trunnion Interface Stress Varies Significantly with Head Size and Activity. *J. Arthroplast.* **2019**, *34*, 157–162. [CrossRef]
188. Harman, M.K.; Banks, S.A.; Hodge, W.A. Wear analysis of a retrieved hip implant with titanium nitride coating. *J. Arthroplast.* **1997**, *12*, 938–945. [CrossRef]
189. Teresa Raimondi, M.; Pietrabissa, R. The in-vivo wear performance of prosthetic femoral heads with titanium nitride coating. *Biomaterials* **2000**, *21*, 907–913. [CrossRef]
190. Taeger, G.; Podleska, L.E.; Schmidt, B.; Ziegler, M.; Nast-Kolb, D. Comparison of Diamond-Like-Carbon and Alumina-Oxide articulating with Polyethylene in Total Hip Arthroplasty. *Mater. Werkst.* **2003**, *34*, 1094–1100. [CrossRef]
191. Cheng, K.; Gopal, V.; McNallan, M.; Manivasagam, G.; Mathew, M.T. Enhanced Tribocorrosion Resistance of Hard Ceramic Coated Ti-6Al-4V Alloy for Hip Implant Application: In-Vitro Simulation Study. *ACS Biomater. Sci. Eng.* **2019**, *5*, 4817–4824. [CrossRef] [PubMed]
192. Tasdemir, M.; Senaslan, F.; Celik, A. Investigation of corrosion and thermal behavior of PU-PDMS-coated AISI 316L. *e-Polymers* **2021**, *21*, 355–365. [CrossRef]
193. Benea, L.; Simionescu, N.; Celis, J.P. Electro-codeposition of CeO₂ nanoparticles into cobalt matrix to improve the tribocorrosion performances of Co/nano CeO₂ composite layers in biological solution for medical applications. *J. Mech. Behav. Biomed. Mater.* **2020**, *101*, 103443. [CrossRef] [PubMed]

194. Esguerra-Arce, J.; Castañeda, A.B.; Esguerra-Arce, A.; Aguilar, Y.; Mischler, S. Fretting corrosion between bone and calcium phosphate-calcium titanate coatings. *Wear* **2018**, *414–415*, 366–375. [[CrossRef](#)]
195. Esfahani, E.; Bukuaghangin, O.; Banfield, S.; Vangolu, Y.; Yang, L.; Neville, A.; Hall, R.; Bryant, M. Surface engineering of wrought and additive layer manufactured Ti-6Al-4V alloy for enhanced load bearing and bio-tribocorrosion applications. *Surf. Coat. Technol.* **2022**, *442*, 128139. [[CrossRef](#)]
196. Anand, A.; Das, M.; Kundu, B.; Balla, V.K.; Bodhak, S.; Gangadharan, S. Tribocorrosion characteristics of Ti₆Al₄V-TiB-TiN in-situ composite coatings prepared using plasma spraying. *J. Compos. Mater.* **2021**, *55*, 1935–1946. [[CrossRef](#)]
197. Zhu, X.; Dang, B.; Li, F.; Wei, D.; Zhang, P.; Li, S. Tribocorrosion behavior of Nb coating deposited by double-glow plasma alloying. *Mater. Res. Express* **2021**, *8*, 016411. [[CrossRef](#)]
198. Gopal, V.; Chandran, M.; Rao, M.S.R.; Mischler, S.; Cao, S.; Manivasagam, G. Tribocorrosion and electrochemical behaviour of nanocrystalline diamond coated Ti based alloys for orthopaedic application. *Tribol. Int.* **2017**, *106*, 88–100. [[CrossRef](#)]
199. López-Ortega, A.; Bayón, R.; Arana, J.L. Evaluation of protective coatings for offshore applications. Corrosion and tribocorrosion behavior in synthetic seawater. *Surf. Coat. Technol.* **2018**, *349*, 1083–1097. [[CrossRef](#)]
200. Sun, X.; Huang, D.; Wu, G. The current state of offshore wind energy technology development. *Energy* **2012**, *41*, 298–312. [[CrossRef](#)]
201. ISO 12944-5:2019; Paints and Varnishes—Corrosion Protection of Steel Structures by Protective Paint Systems—Part 5: Protective Paint Systems. International Organization for Standardization: Geneva, Switzerland, 2019.
202. NORSOK M-501:2022; Surface Preparation and Protective Coating. Standards Norway: Lysaker, Norway, 2022.
203. López-Ortega, A.; Bayón, R.; Arana, J.L. Evaluation of Protective Coatings for High-Corrosivity Category Atmospheres in Offshore Applications. *Materials* **2019**, *12*, 1325. [[CrossRef](#)] [[PubMed](#)]
204. Yan, H.; Cai, M.; Song, S.; Huang, Y.; Fan, X.; Zhu, M. Expounding the interaction of ultraviolet irradiation and tribocorrosion on soap fiber enhanced epoxy coating. *Prog. Org. Coat.* **2022**, *163*, 106604. [[CrossRef](#)]
205. Li, H.; Liu, L.; Guo, P.; Sun, L.; Wei, J.; Liu, Y.; Li, S.; Wang, S.; Lee, K.; Ke, P.; et al. Long-term tribocorrosion resistance and failure tolerable of multilayer carbon-based coatings. *Friction* **2022**, *10*, 1707–1721. [[CrossRef](#)]
206. Liu, Y.; Li, S.; Li, H.; Ma, G.; Sun, L.; Guo, P.; Ke, P.; Lee, K.; Wang, A. Controllable defect engineering to enhance the corrosion resistance of Cr/GLC multilayered coating for deep-sea applications. *Corros. Sci.* **2022**, *199*, 110175. [[CrossRef](#)]
207. Xu, X.; Guo, P.; Zuo, X.; Sun, L.; Li, X.; Lee, K.; Wang, A. Understanding the effect of Al/Ti ratio on the tribocorrosion performance of Al/Ti co-doped diamond-like carbon films for marine applications. *Surf. Coat. Technol.* **2020**, *402*, 126347. [[CrossRef](#)]
208. Kuptsov, K.A.; Antonyuk, M.N.; Bondarev, A.V.; Sheveyko, A.N.; Shtansky, D.V. Electrospark deposition of wear and corrosion resistant Ta(Zr)C-(Fe,Mo,Ni) coatings to protect stainless steel from tribocorrosion in seawater. *Wear* **2021**, *486–487*, 204094. [[CrossRef](#)]
209. Zhang, C.; Lu, X.; Wang, C.; Sui, X.; Wang, Y.; Zhou, H.; Hao, J. Tailoring the microstructure, mechanical and tribocorrosion performance of (CrNbTiAlV)N-x high-entropy nitride films by controlling nitrogen flow. *J. Mater. Sci. Technol.* **2022**, *107*, 172–182. [[CrossRef](#)]
210. Niu, D.; Zhang, C.; Sui, X.; Lu, X.; Zhang, X.; Wang, C.; Hao, J.; Shi, Z. Microstructure, mechanical properties and tribo-corrosion mechanism of (CrNbTiAlVMo)_xN_{1-x} coated 316 L stainless steel in 3.5 wt% NaCl solution. *Tribol. Int.* **2022**, *173*, 107638. [[CrossRef](#)]
211. Wang, Y.; Zhang, J.; Wang, Y.; Wang, C.; Guo, W.; Lu, X.; Sui, Y.; Lan, J. Inhibiting tribocorrosion damage of Cr/Cr_xN coatings by multi-layer design. *Ceram. Int.* **2021**, *47*, 842–850. [[CrossRef](#)]
212. Wang, Y.; Zhang, J.; Zhou, S.; Wang, Y.; Wang, C.; Wang, Y.; Sui, Y.; Lan, J.; Xue, Q. Improvement in the tribocorrosion performance of CrCN coating by multilayered design for marine protective application. *Appl. Surf. Sci.* **2020**, *528*, 147061. [[CrossRef](#)]
213. Zhang, J.; Su, X.; Shan, L.; Liu, Y.; Zhang, P.; Jia, Y. Preparation and tribocorrosion performance of CrCN coatings in artificial seawater on different substrates with different bias voltages. *Ceram. Int.* **2019**, *45*, 9901–9911. [[CrossRef](#)]
214. Shan, L.; Wang, Y.; Zhang, Y.; Zhang, Q.; Xue, Q. Tribocorrosion behaviors of PVD CrN coated stainless steel in seawater. *Wear* **2016**, *362–363*, 97–104. [[CrossRef](#)]
215. Xu, X.; Sun, J.; Xu, Z.; Li, Z.; Su, F. Microstructure, electrochemical and tribocorrosion behaviors of CrCN nanocomposite coating with various carbon content. *Surf. Coat. Technol.* **2021**, *411*, 126997. [[CrossRef](#)]
216. Wang, H.; Ou, Y.; Zhang, X.; Liao, B.; Ou, X.; Luo, J.; Pang, P.; Chen, L.; Hua, Q.; Bao, M. Tribocorrosion behaviors of TiSiCN nanocomposite coatings deposited by high power impulse magnetron sputtering. *Mater. Res. Express* **2020**, *7*, 076407. [[CrossRef](#)]
217. Zeng, Q.; Xu, Y. A comparative study on the tribocorrosion behaviors of AlFeCrNiMo high entropy alloy coatings and 304 stainless steel. *Mater. Today Commun.* **2020**, *24*, 101261. [[CrossRef](#)]
218. Ma, F.; Li, J.; Zeng, Z.; Gao, Y. Tribocorrosion behavior in artificial seawater and anti-microbiologically influenced corrosion properties of TiSiN-Cu coating on F690 steel. *J. Mater. Sci. Technol.* **2019**, *35*, 448–459. [[CrossRef](#)]
219. Ma, F.; Li, J.; Zeng, Z.; Gao, Y. Structural, mechanical and tribocorrosion behaviour in artificial seawater of CrN/AlN nanomultilayer coatings on F690 steel substrates. *Appl. Surf. Sci.* **2018**, *428*, 404–414. [[CrossRef](#)]
220. Alkan, S.; Gök, M.S. Influence of plasma nitriding pre-treatment on the corrosion and tribocorrosion behaviours of PVD CrN, TiN and AlTiN coated AISI 4140 steel in seawater. *Lubr. Sci.* **2022**, *34*, 67–83. [[CrossRef](#)]
221. Cheng, J.; Ge, Y.; Wang, B.; Zhang, L.; Hu, X.; Hong, S.; Liang, X.; Zhang, X. Microstructure and Tribocorrosion Behavior of Al₂O₃/Al Composite Coatings: Role of Al₂O₃ Addition. *J. Therm. Spray Technol.* **2020**, *29*, 1741–1751. [[CrossRef](#)]

222. López-Ortega, A.; Arana, J.L.; Rodríguez, E.; Bayón, R. Corrosion, wear and tribocorrosion performance of a thermally sprayed aluminum coating modified by plasma electrolytic oxidation technique for offshore submerged components protection. *Corros. Sci.* **2018**, *143*, 258–280. [[CrossRef](#)]
223. Ou, Y.; Wang, H.; Hua, Q.; Liao, B.; Ouyang, X. Tribocorrosion behaviors of superhard yet tough Ti-C-N ceramic coatings. *Surf. Coat. Technol.* **2022**, *439*, 128448. [[CrossRef](#)]
224. Wu, D.; Cheng, Q.; Yu, Q.; Guan, Z.; Deng, Y.; Liu, Y. Influence of high hydrostatic pressure on tribocorrosion behavior of HVOF WC-10Co-4Cr coating coupled with Si₃N₄ in artificial seawater. *Int. J. Refract. Met. Hard Mater.* **2022**, *108*, 105936. [[CrossRef](#)]
225. Kuptsov, K.A.; Sheveyko, A.N.; Sidorenko, D.A.; Shtansky, D.V. Electro-spark deposition in vacuum using graphite electrode at different electrode polarities: Peculiarities of microstructure, electrochemical and tribological properties. *Appl. Surf. Sci.* **2021**, *566*, 150722. [[CrossRef](#)]
226. Fu, Y.; Zhou, F.; Zhang, M.; Wang, Q.; Zhou, Z. Structural, mechanical and tribocorrosion performances of CrMoSiN coatings with various Mo contents in artificial seawater. *Appl. Surf. Sci.* **2020**, *525*, 146629. [[CrossRef](#)]
227. Zhang, M.; Zhou, F.; Wang, Q.; Fu, Y.; Zhou, Z. Tribocorrosion characteristics of CrMoSiCN/Ag coatings on Ti6Al4V alloys in seawater. *Ceram. Int.* **2021**, *47*, 31780–31797. [[CrossRef](#)]
228. Fu, Y.; Zhou, F.; Zhang, M.; Wang, Q.; Zhou, Z. Structure and tribocorrosion behavior of CrMoSiCN nanocomposite coating with low C content in artificial seawater. *Friction* **2021**, *9*, 1599–1615. [[CrossRef](#)]
229. Fu, Y.; Zhou, F.; Wang, Q.; Zhang, M.; Zhou, Z. Electrochemical and tribocorrosion performances of CrMoSiCN coating on Ti-6Al-4V titanium alloy in artificial seawater. *Corros. Sci.* **2020**, *165*, 108385. [[CrossRef](#)]
230. Wang, Y.; Li, J.; Dang, C.; Wang, Y.; Zhu, Y. Influence of bias voltage on structure and tribocorrosion properties of TiSiCN coating in artificial seawater. *Mater. Charact.* **2017**, *127*, 198–208. [[CrossRef](#)]
231. Liu, K.; Ma, F.; Lou, M.; Dong, M.; Zhu, Y.; Wang, Y.; Wu, X.; Liu, X.; Li, J. Structure and tribocorrosion behavior of TiAlCN coatings with different Al contents in artificial seawater by multi-arc ion plating. *Surf. Topogr. Metrol. Prop.* **2021**, *9*, 045004. [[CrossRef](#)]
232. Zhu, Y.; Dong, M.; Li, J.; Wang, L. The improved corrosion and tribocorrosion properties of TiSiN/Ag by thermal treatment. *Surf. Coat. Technol.* **2020**, *385*, 125437. [[CrossRef](#)]
233. Dong, M.; Zhu, Y.; Xu, L.; Ren, X.; Ma, F.; Mao, F.; Li, J.; Wang, L. Tribocorrosion performance of nano-layered coating in artificial seawater. *Appl. Surf. Sci.* **2019**, *487*, 647–654. [[CrossRef](#)]
234. Dong, M.; Zhu, Y.; Wang, C.; Shan, L.; Li, J. Structure and tribocorrosion properties of duplex treatment coatings of TiSiCN/nitride on Ti₆Al₄V alloy. *Ceram. Int.* **2019**, *45*, 12461–12468. [[CrossRef](#)]
235. Wang, Y.; Li, J.; Dang, C.; Wang, Y.; Zhu, Y. Influence of carbon contents on the structure and tribocorrosion properties of TiSiCN coatings on Ti6Al4V. *Tribol. Int.* **2017**, *109*, 285–296. [[CrossRef](#)]
236. Kowalski, M.; Stachowiak, A. Tribocorrosion Performance of Cr/CrN Hybrid Layer as a Coating for Machine Components Used in a Chloride Ions Environment. *Coatings* **2021**, *11*, 242. [[CrossRef](#)]
237. Cai, K.; Jiang, B.; Zhang, J.; Su, X. Preparation and Tribocorrosion Performance of Different Si-Doped TiSiN-Ag Coatings on Different Substrates in Seawater. *Coatings* **2021**, *11*, 459. [[CrossRef](#)]
238. Totolin, V.; Pejaković, V.; Csanyi, T.; Hekele, O.; Huber, M.; Rodríguez Ripoll, M. Surface engineering of Ti6Al4V surfaces for enhanced tribocorrosion performance in artificial seawater. *Mater. Des.* **2016**, *104*, 10–18. [[CrossRef](#)]
239. Zhou, X.; Dong, Q.; Zhu, S.; Tao, X.; Wang, Z.; Zhang, B. Exploration of tribocorrosion behavior of Fe-based amorphous coating in simulated seawater. *J. Adhes. Sci. Technol.* **2021**, *37*, 997–1009. [[CrossRef](#)]
240. Liu, E.; Zhang, Y.; Wang, X.; Zeng, Z.; Du, H.; Qin, H. Tribocorrosion behaviors of thermal spraying WC/Ni60 coated 316L stainless steel in artificial seawater. *Ind. Lubr. Tribol.* **2019**, *71*, 741–748. [[CrossRef](#)]
241. Pejakovic, V.; Berger, L.; Thiele, S.; Rojacz, H.; Ripoll, M. Fine grained titanium carbonitride reinforcements for laser deposition processes of 316L boost tribocorrosion resistance in marine environments. *Mater. Des.* **2021**, *207*, 109847. [[CrossRef](#)]
242. Ou, Y.X.; Wang, H.Q.; Liao, B.; Lei, M.K.; Ouyang, X.P. Tribological behaviors in air and seawater of CrN/TiN superlattice coatings irradiated by high-intensity pulsed ion beam. *Ceram. Int.* **2019**, *45*, 24405–24412. [[CrossRef](#)]
243. Alkan, S. Enhancement of marine corrosion and tribocorrosion resistance of offshore mooring chain steel by aluminizing process. *Brodogradnja* **2022**, *73*, 131–159. [[CrossRef](#)]

Disclaimer/Publisher’s Note: The statements, opinions and data contained in all publications are solely those of the individual author(s) and contributor(s) and not of MDPI and/or the editor(s). MDPI and/or the editor(s) disclaim responsibility for any injury to people or property resulting from any ideas, methods, instructions or products referred to in the content.